

See discussions, stats, and author profiles for this publication at: <https://www.researchgate.net/publication/230712903>

Active Site Models for the Cu A Site of Peptidylglycine α -Hydroxylating Monooxygenase and Dopamine β -Monooxygenase

ARTICLE *in* INORGANIC CHEMISTRY · AUGUST 2012

Impact Factor: 4.76 · DOI: 10.1021/ic301272h · Source: PubMed

CITATIONS

25

READS

61

10 AUTHORS, INCLUDING:



Mehmed Z Ertem

Brookhaven National Laboratory

35 PUBLICATIONS 648 CITATIONS

[SEE PROFILE](#)



Nobutaka Fujieda

Osaka University

39 PUBLICATIONS 383 CITATIONS

[SEE PROFILE](#)



Christopher J Cramer

University of Minnesota Twin Cities

531 PUBLICATIONS 23,167 CITATIONS

[SEE PROFILE](#)



Shinobu Itoh

Osaka University

230 PUBLICATIONS 4,972 CITATIONS

[SEE PROFILE](#)

Active Site Models for the Cu_A Site of PHM and D β M

Atsushi Kunishita,[†] Mehmed Z. Ertem,[‡] Yuri Okubo,[†] Tetsuro Tano,[†]
Hideki Sugimoto,[†] Kei Ohkubo,[†] Nobutaka Fujieda,[†] Shuichi Fukuzumi,^{†,¶}
Christopher J. Cramer,^{*,‡} and Shinobu Itoh^{*,†}

[†] Department of Material and Life Science, Division of Advanced Science and Biotechnology,
Graduate School of Engineering, Osaka University, 2-1 Yamada-oka, Suita, Osaka 565-0871,
Japan

[‡] Department of Chemistry and Supercomputing Institute, University of Minnesota, 207
Pleasant St. SE, Minneapolis, MN 55455

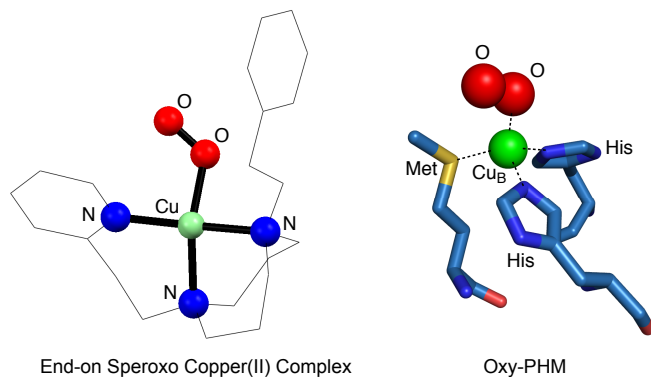
[¶] Department of Bioinspired Science, Ewha Womans University, Seoul 120-750, Korea

*Corresponding Author: shinobu@mls.eng.osaka-u.ac.jp (SI) and cramer@umn.edu (CJC)

ABSTRACT:

A mononuclear copper(II) superoxo species has been invoked as the key reactive intermediate in aliphatic substrate hydroxylation by copper monooxygenases such as peptidylglycine α -hydroxylating monooxygenase (PHM), dopamine β -monooxygenase ($D\beta M$), and tyramine β -monooxygenase ($T\beta M$). We have recently developed a mononuclear copper(II) end-on superoxo complex using a *N*-[2-(2-pyridyl)ethyl]-1,5-diazacyclooctane tridentate ligand, the structure of which is similar to the four-coordinate distorted *tetrahedral* geometry of the copper-dioxygen adduct found in the oxy-form of PHM (Prigge, S. T.; Eipper, B. A.; Mains, R. E.; Amzel, L. M. *Science* **2004**, *304*, 864-867). In this study, structures and physicochemical properties as well as reactivity of the copper(I) and copper(II) complexes supported by a series of tridentate ligands having the same *N*-[2-(2-pyridyl)ethyl]-1,5-diazacyclooctane framework have been examined in detail in order to shed light on the chemistry dictated in the active sites of mononuclear copper monooxygenases. The ligand exhibits unique feature to stabilize the copper(I) complexes in a T-shape geometry and the copper(II) complexes in a distorted tetrahedral geometry. Low temperature oxygenation of the copper(I) complexes generated the mononuclear copper(II) end-on superoxo complexes, the structure and spin state of which have been further characterized by DFT calculations. Detailed kinetic analysis on the O_2 -adduct formation reaction gave the kinetic and thermodynamic parameters providing mechanistic insights into the association and dissociation processes of O_2 to the copper complexes. The copper(II) end-on superoxo complex thus generated gradually decomposed to induce aliphatic ligand hydroxylation. Kinetic and DFT studies on the decomposition reaction have suggested that C-H bond abstraction occurs unimolecularly from the superoxo complex with subsequent rebound of the copper hydroperoxo species to generate the oxygenated product. The present results have indicated that a superoxo species having a four-coordinate distorted *tetrahedral* geometry could be reactive enough to induce the direct C-H bond activation of aliphatic substrates in the enzymatic systems.

TOC Graphic



INTRODUCTION

Dioxygen activation at a mononuclear copper reaction center has attracted much recent attention because of its strong relevance to biological and synthetic oxidation/oxygenation reactions.¹⁻¹² For instance, peptidylglycine α -hydroxylating monooxygenase (PHM), dopamine β -monooxygenase (D β M), and tyramine β -monooxygenase (T β M) have been reported to catalyze aliphatic C–H bond hydroxylation of their respective substrates (dopamine, peptide hormones, and tyramine, respectively) using a mononuclear copper active-oxygen species.^{1,13-16} These enzymes possess a similar active site consisting of two different mononuclear copper reaction centers (designated as Cu_A and Cu_B) separated by ~11 Å.¹⁷ According to the X-ray structure of resting PHM reported by Amzel and his coworkers, Cu_A site exhibits a distorted trigonal planar geometry with three histidine imidazole ligands, whereas Cu_B site has a distorted tetrahedral geometry consisting with two histidine imidazole ligands, one methionine thioether ligand, and a water molecule as shown in Figure 1A.^{18,19}

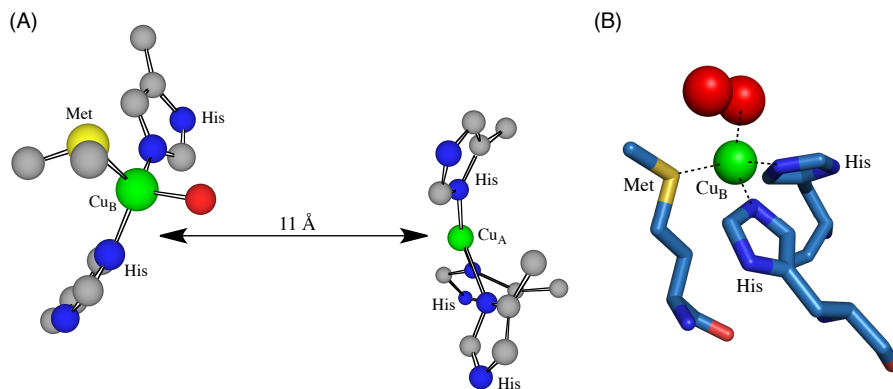


Figure 1. (A) The active site structure of PHM.¹⁷ (B) The copper-superoxo species involved in oxy-PHM.²⁰

It has been suggested that the Cu_A site is associated with electron transfer from ascorbate (physiological reductant) to the Cu_B site acting as the reaction center for dioxygen activation and subsequent substrate hydroxylation. Recently, Amzel and his coworkers also determined the crystal structure of the oxy-form of PHM to demonstrate that Cu_B exhibits a distorted *tetrahedral* geometry including an end-on superoxo species ($\eta^1\text{-O}_2\cdot^-$) as shown in

Figure 1B.²⁰ The recent enzymatic studies as well as the theoretical studies have suggested that the mononuclear copper(II) superoxo species (Figure 1B) could be a key reactive intermediate that is directly involved in the C–H bond activation of the substrates.^{4,13,15,19,21–26} However, little is known about the physicochemical properties and reactivity of such an end-on superoxo copper(II) species having a distorted *tetrahedral* geometry.

In the synthetic modeling studies, a great deal of effort has been made to obtain insights into the structure, physicochemical properties, and reactivity of mononuclear copper(II) active-oxygen complexes.^{27–42} With respect to the mononuclear copper(II)-superoxo complex, Kitajima and co-workers reported the first crystal structure of a *side-on* superoxo copper(II) complex **S^S** supported by a sterically demanding tridentate ligand, which exhibits a five-coordinate *square pyramidal* structure as shown in Figure 2 (left).²⁸ However, it was later found that the reaction of the corresponding copper(I) complex $[\text{Cu}^{\text{I}}(\text{HB}(3\text{-}t\text{Bu}\text{-}5\text{-}i\text{Prpz})_3)]$ with O₂ gave a mixture of the mononuclear copper(II)-superoxo complex and a dinuclear copper(II) side-on peroxy complex, ($\mu\text{-}\eta^2\text{:}\eta^2\text{-peroxy}$)dicopper(II), *in solution*. Thus, they re-examined the spectroscopic features of the mononuclear copper(II) side-on superoxo complex using the more sterically demanding ligand HB(3-Ad-5-iPr-pz)₃⁻ (Ad = adamantyl) to demonstrate that the complex has a diamagnetic ground state ($S = 0$) and exhibits weak absorption bands at 383, 452, 699, and 980 nm with extinction coefficients smaller than 300 M⁻¹ cm⁻¹.²⁹

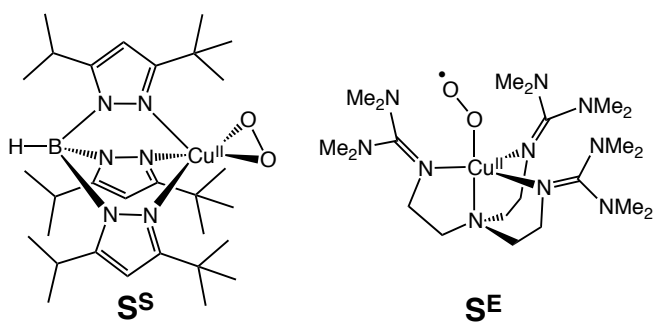


Figure 2. Structurally characterized copper(II)-superoxo complexes: $[\text{Cu}^{\text{II}}(\eta^2\text{-O}_2)(\text{HB}(3\text{-}t\text{Bu}\text{-}5\text{-}i\text{Prpz})_3)]^+$ (**S^S**)²⁸ and $[\text{Cu}^{\text{II}}(\eta^1\text{-O}_2)(\text{TMG}_3\text{tren})]^+$ (**S^E**).³⁵

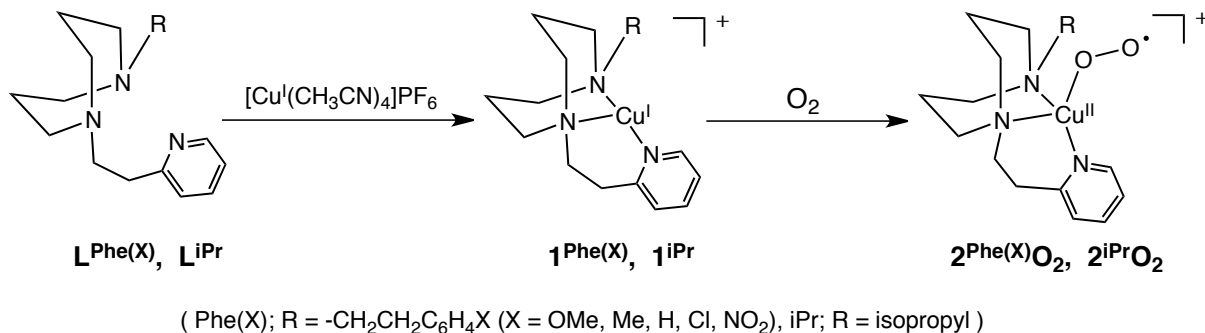
More recently, Schindler *et al.* reported a mononuclear copper(II) *end-on* superoxo complex $[\text{Cu}^{\text{II}}(\eta^1\text{-O}_2)(\text{TMG}_3\text{tren})]^+$ (S^{E}) supported by tris(tetramethylguanidino)tren (TMG₃tren) tetradentate ligand (Figure 2, right).³⁵ In this case, the complex exhibits a five-coordinate *trigonal bipyramidal* geometry with an end-on superoxide as one of the axial ligands. The end-on superoxo complex S^{E} exhibits a relatively intense absorption band at 447 nm ($\epsilon = 3400 \text{ M}^{-1} \text{ cm}^{-1}$) together with broad absorption bands at 680 nm and 780 nm. The NMR analyses and theory clearly indicated that the compound has a triplet ground state ($S = 1$).⁴⁰

With respect to reactivity of the mononuclear copper(II) superoxo complexes, no experimental data is available for the Kitajima's side-on superoxo complex, $[\text{Cu}^{\text{II}}(\eta^2\text{-O}_2)([\text{HB}(3\text{-}t\text{Bu-5-}i\text{Prpz})_3])]^+$ (S^{S}). On the other hand, the end-on superoxo complex, $[\text{Cu}^{\text{II}}(\eta^1\text{-O}_2)(\text{TMG}_3\text{tren})]^+$ (S^{E}), has been shown to react with hydrogen atom donors such as phenols and TEMPO-H (2,2,6,6-tetramethylpyperidine-1-hydroxide) to generate a hydroperoxo intermediate $\text{LCu}^{\text{II}}\text{OOH}$.³⁷ In this case, they observed aliphatic ligand hydroxylation of one of the methyl groups of the tetramethylguanidino substituent.³⁷ The same ligand hydroxylation took place, when the copper(II) complex of the same ligand was reacted with H_2O_2 in the presence of a base or the copper(I) complex was treated with PhIO .³⁷ However, decomposition of the superoxo complex itself did not afford the hydroxylated product.³⁷ On the basis of these results, they concluded that the end-on superoxo complex itself was not directly involved in the aliphatic C–H bond activation, but instead a putative copper(II) oxyl radical species $\text{LCu}^{\text{II}}\text{O}^{\cdot}$ generated by O–O bond homolysis of the hydroperoxo complex $\text{LCu}^{\text{II}}\text{OOH}$ may be the real active-oxygen species.³⁷

Recently, we have succeeded to develop a new type of end-on superoxo copper(II) complex $\text{2}^{\text{Phe(X)}}\text{O}_2$ having a four-coordinate distorted *tetrahedral* geometry (Scheme 1).⁴³ The structure of $\text{2}^{\text{Phe(X)}}\text{O}_2$ is more similar to the suggested structure of the active oxygen species of PHM (Figure 1B) as compared to Schindler's end-on superoxo complex S^{E} having trigonal bipyramidal structure (Figure 2).⁴³ The compound is generated by the reaction of copper(I) complexes supported by *tridentate* ligand $\text{L}^{\text{Phe(X)}}$ (Chart 1, X = OMe, H, NO₂) with O₂ at low

temperature (Scheme 1).⁴³ The superoxo complex has been characterized by UV-vis [$\lambda_{\text{max}} = 397 \text{ nm}$ ($\epsilon = 4200 \text{ M}^{-1} \text{ cm}^{-1}$), 570 (850), and 705 (1150)] and resonance Raman spectroscopic methods ($\nu_{\text{O}-\text{O}} = 1033$ and $\nu_{\text{Cu}-\text{O}} = 457 \text{ cm}^{-1}$, shift to 968 and 442 cm^{-1} , respectively, upon $^{18}\text{O}_2$ substitution).⁴³ Moreover, the superoxo complex $\mathbf{2}^{\text{Phe(X)}}\text{O}_2$ has been shown to have a triplet ground state ($S = 1$) as confirmed by EPR and to exhibit aliphatic ligand hydroxylation reactivity.⁴³

Scheme 1. Formation of End-on Superoxide Copper(II) Complex $\mathbf{2}^{\text{R}}\text{O}_2$



Our success may rely on the unique structural feature of the supporting ligand, *N*-[2-(2-pyridyl)ethyl]-1,5-diazacyclooctane derivative, which enforces the copper(II) complexes taking a mononuclear structure with a distorted tetrahedral geometry. So far, *N*-substituted 1,5-diazaoctane (DACO) derivative ligands have been demonstrated to provide copper(II) complexes having structural features deviating from the normal tetragonal geometry of copper(II).^{38,44-48} In this study, the structure, physicochemical properties, and reactivity of the copper(I) and copper(II) complexes including the superoxo complexes $\mathbf{2}^{\text{R}}\text{O}_2$ supported by $\mathbf{L}^{\text{Phe(X)}}$ and \mathbf{L}^{iPr} (Scheme 1) have been examined in detail in order to shed light on the chemistry of resting states, reduced states, and oxidized states of the enzymes.

■ EXPERIMENTAL SECTION

Materials and Methods. The reagents and the solvents used in this study, except the

ligands and the copper complexes, were commercial products of the highest available purity and were further purified by the standard methods, if necessary.⁴⁹ Ligands 1-(2-phenethyl)-5-[2-(2-pyridyl)ethyl]-1,5-diazacyclooctane ($\text{L}^{\text{Phe(H)}}$), 1-[2-(4-nitrophenyl)-ethyl]-5-[2-(2-pyridyl)ethyl]-1,5-diazacyclooctane ($\text{L}^{\text{Phe(NO}_2)}$), and 1-[2-(4-methoxyphenyl)-ethyl]-5-[2-(2-pyridyl)ethyl]-1,5-diazacyclooctane ($\text{L}^{\text{Phe(OMe)}}$) and their copper(I) complexes ($\text{1}^{\text{Phe(H)}}$, $\text{1}^{\text{Phe(NO}_2)}$, and $\text{1}^{\text{Phe(OMe)}}$) and copper(II) complexes ($\text{2}^{\text{Phe(NO}_2)}\text{Cl}$ and $\text{2}^{\text{Phe(NO}_2)}\text{OAc}$) were prepared according to the reported procedures.⁴³ FT-IR spectra were recorded on a Jasco FTIR-4100, and UV-visible spectra were taken on a Hewlett Packard 8453 photo diode array spectrophotometer equipped with a Unisoku thermostated cell holder USP-203 designed for low temperature measurements. $^1\text{H-NMR}$ spectra were recorded on a JEOL LMN-ECP300WB, a JEOL ECP400, a JEOL ECS400, or a Varian UNITY INOVA 600MHz spectrometer. ESI-MS (electrospray ionization mass spectra) measurements were performed on a PE SCIEX API 150EX, a PerSeptive Biosystems MarinerTM Biospectrometry workstation, or a Micromass LCT spectrometer.

Dioxygen concentrations in organic solvents (acetone, THF, and propionitrile) at various temperature ($-70 \sim -90^\circ\text{C}$) were calculated by using the equation, $C_T = C_0 (d_T/d_0)$, where C_T and d_T are the O_2 concentration and the density of solution at temperature T, and C_0 and d_0 are the known values at room temperature.⁵⁰ Because of the small solubility of O_2 in liquids, the density of the solution can be assumed equal to that of pure solvent. For several common solvents, densities were experimentally determined in a wide range of temperatures and fit satisfactorily with the following equation, $d_T = a - bT$ (T in K; the parameters a and b are found in the literatures).⁵¹

1-[2-(4-Methylphenyl)ethyl]-1,5-diazacyclooctane. A mixture of DACO (1,5-diazacyclooctane)•2HBr (7.0 g, 25 mmol) and KOH (2.8 g, 50 mmol) in $\text{CH}_3\text{CN-H}_2\text{O}$ (5 : 1, 120 mL) was stirred for 1 h at room temperature. Then, 2-(4-methylphenyl)ethyl bromide (5.0 g, 25 mmol) and triethylamine (13 g, 100 mmol) were added to the solution, and the resulting solution was refluxed for 14 h. The solvent was removed under reduced pressure, and the resulting residue was dissolved in water (10 mL), to which NaOH(aq) was added

slowly until the pH of the solution became 14. The aqueous solution was extracted with CHCl_3 (20 mL x 3), and the combined organic layer was dried over Na_2SO_4 . After removal of Na_2SO_4 by filtration, evaporation of the solvent gave dark brown oil. Purification by Kugelrohr distillation (200 °C, 5.0 Torr) afforded the pure product as a colorless oil in a 19 % isolated yield. $^1\text{H-NMR}$ (CDCl_3 , 300 MHz) δ 1.61 (4 H, pentet, $J = 5.7$ Hz, $-\text{CH}_2-$), 2.31 (3 H, s, $-\text{CH}_3$), 2.57–2.71 (8 H, m, $-\text{CH}_2-$), 2.84 (4 H, t, $J = 5.7$ Hz, $-\text{CH}_2-$), 7.09 (4 H, br s, ArH); HRMS (FAB $^+$) m/z = 232.1933, calcd for $\text{C}_{15}\text{H}_{24}\text{N}_2$ = 232.1940.

1-[2-(4-Methylphenyl)ethyl]-5-[2-(2-pyridyl)ethyl]-1,5-diazacyclooctane

($\text{L}^{\text{Phe(Me)}}$). To a methanol solution (40 mL) containing 1-[2-(4-methylphenyl)ethyl]-1,5-diazacyclooctane (680 mg, 3.1 mmol) and 2-vinylpyridine (1.5 g, 15.5 mmol) was added acetic acid (1.0 g, 15.5 mmol), and the mixture was refluxed for 1 day. Removal of the solvent by evaporation gave brown oil, from which ligand $\text{L}^{\text{Phe(Me)}}$ was isolated by alumina column chromatography (eluent: AcOEt) in 56 %. $^1\text{H-NMR}$ (CDCl_3 , 300 MHz) δ 1.65 (4 H, pentet, $J = 5.7$ Hz, $-\text{CH}_2-$), 2.31 (3 H, s, $-\text{CH}_3$), 2.72–2.79 (12 H, m, $-\text{CH}_2-$), 2.93 (4 H, s, $-\text{CH}_2-$), 7.09–7.19 (6 H, m, ArH), 7.57 (1 H, dt, $J = 1.8$ Hz and $J = 7.5$ Hz, PyH₄), 8.52 (1 H, d, $J = 4.8$ Hz, PyH₆); HRMS (FAB $^+$) m/z = 338.2603, calcd for $\text{C}_{22}\text{H}_{32}\text{N}_3$ = 338.2596.

1-[2-(4-Chlorophenyl)ethyl]-1,5-diazacyclooctane. This compound was

prepared by a similar procedure as described for the synthesis of 1-[2-(4-methylphenyl)ethyl]-1,5-diazacyclooctane using 2-(4-chlorophenyl)ethyl bromide instead of (2-(4-methylphenyl)ethyl bromide in a 14 % isolated yield. $^1\text{H-NMR}$ (CDCl_3 , 300 MHz) δ 1.61 (4 H, pentet, $J = 5.7$ Hz, $-\text{CH}_2-$), 2.63–2.76 (8 H, m, $-\text{CH}_2-$), 2.84 (4 H, t, $J = 5.7$ Hz, $-\text{CH}_2-$), 7.12 (2 H, d, $J = 8.4$ Hz, ArH), 7.25 (2 H, d, $J = 8.4$ Hz, ArH); HRMS (FAB $^+$) m/z = 253.1474, calcd for $\text{C}_{14}\text{H}_{22}\text{N}_2\text{Cl}_1$ = 253.1472.

1-[2-(4-Chlorophenyl)ethyl]-5-[2-(2-pyridyl)ethyl]-1,5-diazacyclooctane

($\text{L}^{\text{Phe(Cl)}}$). This compound was prepared by a similar procedure as described for the synthesis of $\text{L}^{\text{Phe(Me)}}$ using 1-[2-(4-chlorophenyl)ethyl]-1,5-diazacyclooctane instead of 1-[2-(4-methylphenyl)- ethyl]-1,5-diazacyclooctane in 65 %. $^1\text{H-NMR}$ (CDCl_3 , 300 MHz) δ 1.64 (4 H, pentet, $J = 5.7$ Hz, $-\text{CH}_2-$), 2.71–2.77 (12 H, m), 2.92 (4 H, s), 7.07–7.26 (6 H, m,

ArH) 7.58 (1 H, td, J = 1.6 Hz and J = 7.5 Hz, PyH₄), 8.52 (1 H, d, J = 4.2 Hz, PyH₆); HRMS (FAB⁺) m/z = 357.1972, calcd for C₂₁H₂₈Cl₁N₃ = 357.1975.

1-Isopropyl-5-[2-(2-pyridyl)ethyl]-1,5-diazacyclooctane (L^{iPr}). 1-Isopropyl-1,5-diazacyclooctane was prepared according to the reported procedures.⁵² To a methanol solution (20 mL) containing 1-isopropyl-1,5-diazacyclooctane (0.33 g, 2.1 mmol) and 2-vinilpyridine (0.67 g, 6.3 mmol) was added acetic acid (0.38 g, 6.3 mmol), and the mixture was refluxed for 2 days. The solvent was removed by evaporation and the resulting residue was dissolved in water (15 mL), to which NaOH(aq) was added slowly until the pH of the solution become 14. The aqueous solution was extracted with CH₂Cl₂(20 mL x 5), and the combined organic layer was dried over Na₂SO₄. After removal of Na₂SO₄ by filtration, the solvent was evaporated to give a brown oil, from which L^{iPr} was isolated by alumina column chromatography (eluent: from AcOEt : hexane = 1 : 1 to AcOEt only) in 77 %. ¹H-NMR (CDCl₃, 600 MHz) δ 0.98 (6 H, d, J = 6.8 Hz), 1.65 (4 H, pentet, J = 6.0 Hz), 2.74 (4 H, t, J = 6.0 Hz), 2.84 (4 H, t, J = 6.0 Hz), 3.00 (4 H, m), 3.12 (1 H, septet, J = 6.8 Hz), 7.10 (1 H, ddd, J = 7.6, 5.0, and 1.1 Hz), 7.19 (1 H, br d, J = 7.6 Hz), 7.58 (1 H, td, J = 7.6 and 1.1 Hz), 8.52 (1 H, ddd, J = 5.0, 1.9, and 0.9 Hz); HRMS (FAB, pos): m/z = 262.2274. Calcd for C₁₆H₂₈N₃ 262.2283.

[Cu^I(L^{Phe(Me)})](PF₆) (1^{Phe(Me)}). Ligand L^{Phe(Me)} (67.4 mg, 0.2 mmol) was treated with an equimolar amount of [Cu^I(CH₃CN)₄]PF₆ (74.0 mg, 0.2 mmol) in CH₂Cl₂-CH₃CN (7 : 1, 4 mL) under Ar atmosphere in a glove box. After stirring the mixture for 5 min at room temperature, insoluble material was removed by filtration. Addition of ether (100 mL) to the filtrate gave a pale yellow powder that was precipitated by standing the mixture for several minutes. The supernatant was then removed by decantation, and the remained pale yellow solid was washed with ether three times and dried to give complex 1^{Phe(Me)} in 62 %. Single crystals of 1^{Phe(Me)} were obtained by vapor diffusion of ether into a CH₂Cl₂-CH₃CN (10 : 1) solution of the complex. FT-IR (KBr) 840 cm⁻¹ (PF₆⁻); HRMS (FAB⁺): m/z 400.1813, calcd for C₂₂H₃₁CuN₃ 400.1814; Anal. Calcd for [Cu^I(L^{Phe(Me)})]PF₆·H₂O (C₂₂H₃₃CuF₆N₃O₁P₁): C, 46.85; H, 5.90; N, 7.45. Found: C, 46.64; H, 5.50; N, 7.77.

[Cu^I(L^{Phe(Cl)})(PF₆) (1^{Phe(Cl)})]. This compound was prepared by a similar procedure as described for the synthesis of 1^{Phe(Me)} in 51 % using L^{Phe(Cl)} instead of L^{Phe(Me)}. Single crystals of 1^{Phe(Cl)} were obtained by diffusion of *n*-hexane into a CH₂Cl₂-CH₃CN (10 : 1) solution of the complex. FT-IR (KBr) 840 cm⁻¹ (PF₆⁻); HRMS (FAB⁺): *m/z* 420.1279, calcd for C₂₁H₂₈CuN₃Cl₁ 420.1267; Anal. Calcd for [Cu^I(L^{Phe(Cl)})]PF₆·H₂O (C₂₁H₂₈CuF₆N₃Cl₁P₁): C, 44.63; H, 4.99; N, 7.39. Found: C, 44.53; H, 4.98; N, 7.42.

[Cu^I(L^{iPr})(PF₆) (1^{iPr})]. To an acetonitrile solution (30 mL) containing L^{iPr} (50 mg, 0.19 mmol) was added [Cu^I(CH₃CN)₄]PF₆ (71 mg, 0.19 mmol), when the color of the solution was turned light green. After stirring 5 min, volume of the solvent was reduced under reduced pressure, and diethyl ether (5 mL) was added to the residue to give light green powder of the product (69 mg, 76 %). Single crystal was obtained by vapor diffusion of ether into a CH₃CN solution of the complex. Anal. Calcd for [Cu^I(L^{iPr})]PF₆·0.05[Cu(CH₃CN)₄]PF₆ (C_{16.4}H_{27.6}Cu_{1.05}F_{6.3}N_{3.2}P_{1.05}): C, 40.32; H, 5.69; N, 9.17. Found: C, 40.28; H, 5.40; N, 8.96; ESI-MS (pos) *m/z* = 324.2 calcd for: C₁₆H₂₇BCuN₆: 324.2

[Cu^{II}(L^{Phe(NO₂)})(NO₂)](BF₄) (2^{Phe(NO₂)NO₂}). Ligand L^{Phe(NO₂)} (50 mg, 0.14 mmol) was treated with an equimolar amount of Cu^{II}SO₄·5H₂O (34 mg, 0.14 mmol) in CH₃OH (20 mL). After stirring the mixture for 3 min at room temperature. NaNO₂ (12 mg, 0.18 mmol) and NH₄BF₄ (42 mg, 0.40 mmol) were added to the solution continuously. Insoluble material was then removed by filtration. Addition of ether (100 mL) to the filtrate gave a blue powder that was precipitated by standing the mixture for several minutes. The supernatant was then removed by decantation, and the remained blue solid was washed with ether three times and dried to give complex in 87 %. Single crystals of 2^{Phe(NO₂)NO₂} were obtained by vapor diffusion of hexane into CH₂Cl₂ solution of the complex. FT-IR (KBr) 1053 cm⁻¹ (BF₄⁻); Anal. Calcd for [Cu^{II}(L^{Phe(NO₂)})(NO₂)](BF₄)·H₂O (C₂₂H₃₂BCuF₄N₅O₅): C, 43.27; H, 5.19; N, 12.02. found: C, 43.54; H, 5.16; N, 12.08.

[Cu^{II}(L^{iPr})(OAc)](BF₄) (2^{iPrOAc}). To an ethanol solution (30 mL) containing L^{iPr} (59 mg, 0.22 mmol) was added Cu(OAc)₂·H₂O (45 mg, 0.22 mmol), when the color of the solution was turned dark blue. After stirring 5 minutes, NH₄BF₄ (70 mg, 0.67 mmol) was

added to the solution and the mixture was stirred for 2 minutes. Volume of the solvent was reduced under reduced pressure to give blue powder, which was collected by filtration and dried (73 mg, 69 %). Single crystals were obtained by vapor diffusion of ether into an acetone solution of the complex. FT-IR (KBr) 1608 cm⁻¹ (C=O), 1055 cm⁻¹ (BF₄⁻); Anal. Calcd for: [Cu^{II}(L^{iPr})(OAc)]BF₄·0.5H₂O (C₁₈H₃₁BCuF₄N₃O_{2.5}): C, 45.06; H, 6.51; N, 8.76; Found: C, 45.01; H, 6.21; N, 8.95; ESI-MS (pos) *m/z* = 382.8 calcd for: C₁₈H₃₀CuN₃O₂: 383.2.

[Cu^{II}(L^{iPr})(N₃)](BF₄) (**2^{iPr}N₃**). To an methanol solution (30 mL) containing L^{iPr} (50 mg, 0.19 mmol) was added CuSO₄·5H₂O (48 mg, 0.19 mmol), when the color of the solution turned dark blue. After stirring for 5 minutes, NaN₃ (16 mg, 0.25 mmol) was then added to give a green solution. After stirring for 2 minutes, NH₄BF₄ (70 mg, 0.67 mmol) was added to the solution and the mixture was stirred for additional 2 minutes. Volume of the solvent was reduced under reduced pressure to give dark green powder, which was collected by filtration and dried (69 mg, 80 %). Single crystals were obtained by vapor diffusion of ether into an acetone solution of the complex. FT-IR (KBr) 2037 cm⁻¹ (N₃⁻), 1057 cm⁻¹ (BF₄⁻); Anal. Calcd for: [Cu^{II}(L^{iPr})(N₃)]BF₄ (C₁₆H₂₇BCuF₄N₆): C, 42.35; H, 6.00; N, 18.52. Found: C, 42.29; H, 5.74; N, 18.25; ESI-MS (pos) *m/z* = 324.2 calcd for: C₁₆H₂₇CuN₃: 324.2.

[Cu^{II}(L^{iPr})(Cl)](PF₆) (**2^{iPr}Cl**). To an ethanol solution (50 mL) containing L^{iPr} (70 mg, 0.27 mmol) was added CuCl₂ (36 mg, 0.27 mmol), when the color of the solution turned greenish blue. After stirring for 5 minutes, NH₄PF₆ (130 mg, 0.81 mmol) was added to the solution and the mixture was stirred for additional 2 minutes. Volume of the solvent was reduced under reduced pressure to give green powder, which was collected by filtration and dried (96 mg, 71 %). FT-IR (KBr) 841 cm⁻¹ (PF₆⁻); Anal. Calcd for: [Cu^{II}(L^{iPr})Cl]PF₆·0.5H₂O (C₁₆H₂₈ClCuF₆N₃O_{0.5}P): C, 37.36; H, 5.49; N, 8.17; Found: C, 37.65; H, 5.32; N, 7.85; ESI-MS (pos) *m/z* = 359.1 calcd for: C₁₆H₂₇ClCuN₃: 359.1. Single crystals of **2^{iPr}Cl** was obtained as a BPh₄ salt [Cu^{II}(L^{iPr})(Cl)](BPh₄) by adding NaBPh₄ into a CH₄CN solution of the PF₆ salt [Cu^{II}(L^{iPr})(Cl)](PF₆) obtained above.

[Cu^{II}(L^{iPr})(NO₂)](BF₄) (**2^{iPr}NO₂**). This compound was prepared as blue powder by a similar procedure described for the synthesis of **2^{iPr}N₃** by using NaNO₂ instead of NaN₃(79 %).

Single crystals were obtained by vapor diffusion of ether into an acetone solution of the complex. FT-IR (KBr) 1046 cm⁻¹ (BF₄⁻), Anal. Calcd for: [Cu^{II}LNO₃]PF₆·0.4H₂O (C₁₆H_{27.8}BCuF₄N₄O_{2.4}): C, 41.33; H, 6.03; N, 12.05. Found: C, 41.56; H, 5.83; N, 11.78; ESI-MS (pos) *m/z* = 324.2 calcd for: C₁₆H₂₇CuN₃: 324.2.

X-ray Structure Determination. Each single crystal obtained was mounted on a loop with a mineral oil, and all X-ray data were collected on a Rigaku R-AXIS RAPID diffractmeter using filtered Mo-K α radiation. The structures were solved by direct methods (SIR 2008) and expanded using Fourier techniques. The non-hydrogen atoms were refined anisotropically by full-matrix least squares on F^2 . The hydrogen atoms were attached at idealized positions on carbon atoms and were not refined. All structures in the final stages of refinement showed no movement in the atom positions. The calculations were performed using Single-Crystal Structure Analysis Software, version 3.8. Crystallographic parameters are summarized in Table 1. Atomic coordinates, thermal parameters, and intramolecular bond distances and angles are deposited in the supplementary materials (CIF file format).

EPR Measurements. EPR spectra of copper(II) complexes were recorded on a JEOL X-band spectrometer (JES-RE1XE) with an attached variable temperature apparatus. The EPR spectra were measured in frozen acetone at 77 K. The magnitude of modulation was chosen to optimize the resolution and the signal-to-noise (S/N) ratio of the observed spectra under non-saturating microwave conditions. The *g* values and the hyperfine coupling constants were calibrated with a Mn²⁺ marker.

Kinetic Measurements. Kinetic measurements for the oxygenation reaction of copper(I) complexes, **1**^{Phe(X)} (X = OMe, Me, H, Cl, NO₂) and **1**^{iPr}, and the decomposition reaction of the generated copper(II) superoxo complexes, **2**^{Phe(X)}O₂, and **2**^{iPr}O₂, were performed using a Hewlett Packard 8453 photo diode array spectrophotometer with a Unisoku thermostated cell holder designed for low temperature measurements (USP-203, a desired temperature can be fixed within ± 0.5 °C) in an appropriate solvent (3 mL) at low temperature. The pseudo-first-order rate constants for the formation and decomposition of the copper(II) superoxo complexes were determined from the plots of ln(Δ*A*) vs time based on the time

course of the absorption change at λ_{\max} due to the copper(II) superoxo complexes.

Computational Methods. All geometries were fully optimized at the M11-L⁵³ level of density functional theory using the Stuttgart [8s7p6d | 6s5p3d] ECP10MWB contracted pseudopotential basis set on Cu⁵⁴ and the 6-31G(d) basis set⁵⁵ on all other atoms. In addition, 3 uncontracted f functions having exponents 5.100, 1.275, and 0.320 were placed on Cu. The grid=ultrafine option in Gaussian 09⁵⁶ (see Ref (1) in Supporting Information for full citation of Ref 56) was chosen for integral evaluation and an automatically generated density-fitting basis set was used within the resolution-of-the-identity approximation for the evaluation of Coulomb integrals. The nature of all stationary points was verified by analytic computation of vibrational frequencies, which were also used for the computation of zero-point vibrational energies, molecular partition functions (with all frequencies below 50 cm⁻¹ replaced by 50 cm⁻¹ when computing free energies), and for determining the reactants and products associated with each transition-state structure (by following the normal modes associated with imaginary frequencies). Partition functions were used in the computation of 298 K thermal contributions to free energy employing the usual ideal-gas, rigid-rotator, harmonic oscillator approximation.⁵⁷ Solvation effects associated with acetone as solvent were accounted for by using the SMD continuum solvation model.⁵⁸ Free energy contributions were added to single-point M11-L electronic energies computed with the SDD basis set on Cu and the 6-311+G(2df,p) basis set on all other atoms to arrive at final, composite free energies.

Addition of triplet molecular oxygen to the closed shell singlet Cu(I) complexes may in principle generate either open shell singlet or triplet products. These species were characterized by weak coupling between two different spin centers, and the singlet states were thus not well described by a single determinant as is implicit in the standard Kohn-Sham density functional formalism. In such instances, Kohn-Sham DFT is not directly applicable,^{57,59-61} and we adopt the Yamaguchi broken-spin-symmetry (BS) procedure^{62,63} to compute the energy of the spin-purified low-spin (LS) state as

$$LS_E = \frac{BS_E \left(HS \langle S^2 \rangle - LS \langle S^2 \rangle \right) - HS_E \left(BS \langle S^2 \rangle - LS \langle S^2 \rangle \right)}{HS \langle S^2 \rangle - BS \langle S^2 \rangle}$$

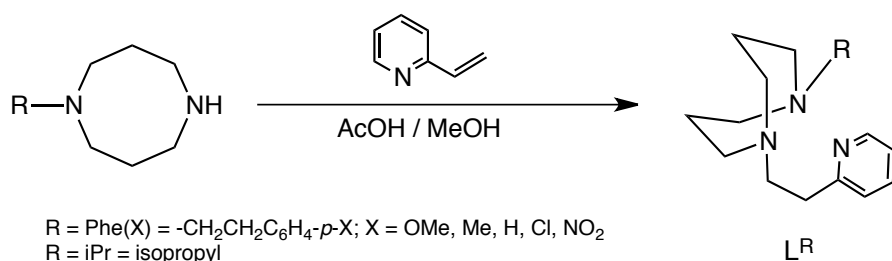
where HS refers to the single-determinantal high-spin coupled state that is related to the low-spin state by spin flip(s) and $\langle S^2 \rangle$ is the expectation value of the total spin operator applied to the appropriate determinant. This broken-symmetry DFT approach has routinely proven effective for the prediction of state-energy splittings in metal coordination compounds.⁶⁴⁻⁶⁷ Time-dependent density functional theory (TDDFT) calculations were performed to predict the UV/visible electronic excitations of postulated intermediates. The B3LYP⁶⁸ density functional, the Stuttgart [8s7p6d + 6s5p3d] ECP10MWB contracted pseudopotential basis set on Cu, and the 6-311+G(d) basis set⁵⁵ on all other atoms were used for the TDDFT calculations with G09 default non-equilibrium solvation effects computed using the SMD continuum solvation model for acetonitrile or acetone as solvent.⁶⁹

■ RESULTS AND DISCUSSION

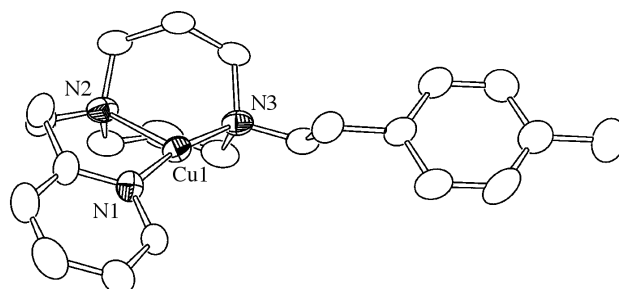
Synthesis and Characterization

Copper(I) Complexes. The tridentate ligands $L^{Phe(X)}$ ($X = OMe, Me, H, Cl, NO_2$) were prepared by Michael addition of 1-(2-*p*-substituted-phenethyl)-1,5-diazacyclooctane to 2-vinylpyridine in refluxing methanol in the presence of excess amount of acetic acid.⁷⁰ Ligand L^{iPr} was prepared in a similar manner by using 1-isopropyl-1,5-diazacyclooctane instead of the *p*-substituted phenetyl derivative as indicated in Scheme 2.

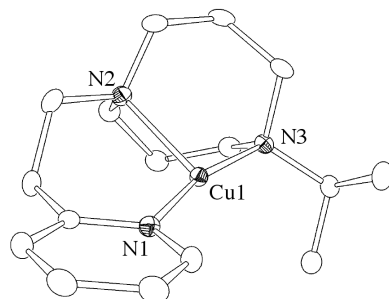
Scheme 2. Synthesis of Supporting Ligands L^R



Treatment of the ligand with $[\text{Cu}^{\text{l}}(\text{CH}_3\text{CN})_4](\text{PF}_6)$ in $\text{CH}_3\text{CN}-\text{CH}_2\text{Cl}_2$ under anaerobic conditions gave the corresponding mononuclear copper(I) complex, $\mathbf{1}^{\text{Phe}(\text{X})}$ and $\mathbf{1}^{\text{iPr}}$. The crystal structures of $\mathbf{1}^{\text{Phe}(\text{OMe})}$, $\mathbf{1}^{\text{Phe}(\text{H})}$, and $\mathbf{1}^{\text{Phe}(\text{NO}_2)}$ have already been reported in our previous communication,⁴³ and those of $\mathbf{1}^{\text{Phe}(\text{Me})}$, $\mathbf{1}^{\text{Phe}(\text{Cl})}$, and $\mathbf{1}^{\text{iPr}}$ have been determined in this study as shown in Figure 3 ($\mathbf{1}^{\text{Phe}(\text{Me})}$ and $\mathbf{1}^{\text{iPr}}$) and Figure S1 ($\mathbf{1}^{\text{Phe}(\text{Cl})}$). The crystallographic data and the selected bond lengths and angles are summarized in Tables 1 and 2 for $\mathbf{1}^{\text{Phe}(\text{Me})}$ and $\mathbf{1}^{\text{iPr}}$ and Tables S1 and S2 for $\mathbf{1}^{\text{Phe}(\text{Cl})}$, respectively.



(A)



(B)

Figure 3. ORTEP drawings of (A) $\mathbf{1}^{\text{Phe(Me)}}$ and (B) $\mathbf{1}^{\text{iPr}}$ showing 50 % probability thermal ellipsoids. The counter anion and the hydrogen atoms are omitted for clarity.

Table 1. X-ray Crystallographic Data of Copper(I) Complexes **1^{Phe(Me)}** and **1^{iPr}**

Compound	1^{Phe(Me)}	1^{iPr}
formula	C ₂₂ H ₃₁ N ₃ CuPF ₆	C ₁₆ H ₂₇ N ₃ CuPF ₆
formula weight	546.02	469.92
crystal system	monoclinic	orthorhombic
space group	<i>P2</i> ₁ /c (#14)	<i>Pbca</i> (#61)
<i>a</i> , Å	7.805(9)	10.6388(4)
<i>b</i> , Å	19.739(17)	13.7319(5)
<i>c</i> , Å	15.504(17)	26.100(1)
α , deg	90	90
β , deg	94.66(5)	90
γ , deg	90	90
<i>V</i> , Å ³	2381(4)	3813.0(3)
<i>Z</i>	4	8
<i>F</i> (000)	1128.00	1936.00
<i>D</i> _{calcd} , g/cm ³	1.523	1.637
<i>T</i> , K	153	103
crystal size, mm	0.40 x 0.30 x 0.20	0.20 x 0.10 x 0.10
μ (MoK α), cm ⁻¹	10.468	12.921
2 θ _{max} , deg	54.9	55.0
no. of reflns measd	21644	34770
no. of reflns obsd	5402 (All reflections)	4364 (All reflections)
no. of variables	329	244
<i>R</i> 1 ^a	0.0487	0.0261
<i>wR</i> 2 ^b	0.0761	0.0588
GOF	1.003	1.008

^a RI = $\sum |F_o| - |F_c| / \sum |F_o|$. ^b wR2 = [$\sum w (|F_o|^2 - |F_c|^2)^2 / \sum w (F_o^2)^2$]^{1/2}

Table 2. Selected Bond Lengths (\AA) and Angles (deg) of $\mathbf{1}^{\text{Phe(Me)}}$ and $\mathbf{1}^{\text{iPr}}$

$\mathbf{1}^{\text{Phe(Me)}}$			
Cu(1)–N(1)	1.899(3)	Cu(1)–N(2)	2.184(4)
Cu(1)–N(3)	1.968(4)		
N(1)–Cu(1)–N(2)	101.30(14)	N(1)–Cu(1)–N(3)	168.27(14)
N(2)–Cu(1)–N(3)	90.33(14)		
$\mathbf{1}^{\text{iPr}}$			
Cu(1)–N(1)	1.9080(14)	Cu(1)–N(2)	2.1783(13)
Cu(1)–N(3)	1.9865(14)		
N(1)–Cu(1)–N(2)	103.15(6)	N(1)–Cu(1)–N(3)	165.82(6)
N(2)–Cu(1)–N(3)	90.62(5)		

All the copper(I) complexes $\mathbf{1}^{\text{Phe(X)}}$ ($X = \text{OMe}$, Me , H , Cl , and NO_2) and $\mathbf{1}^{\text{iPr}}$ exhibit a similar three-coordinate T-shape structure ligated by the three nitrogen atoms N(1), N(2), and N(3) of the supporting ligand.⁴³ The sum of the three angles around the copper center [$\angle \text{N(1)}\text{–Cu(1)}\text{–N(2)}$, $\angle \text{N(1)}\text{–Cu(1)}\text{–N(3)}$, and $\angle \text{N(2)}\text{–Cu(1)}\text{–N(3)}$] is equal to 360° , indicating that the copper ion and the three nitrogen atoms exist in the same plane. It should be noted that the copper(I) complexes do *not* involve a CH_3CN molecule as an external co-ligand even though the complexes were prepared using $[\text{Cu}^{\text{I}}(\text{CH}_3\text{CN})_4]^+$ as the metal source and were crystallized in a CH_3CN -containing solvent (see Experimental Section). In general, copper(I) complexes with an ordinary didentate or tridentate ligand do involve one or more CH_3CN external co-ligand(s) so as to take on a favorable tetrahedral geometry (assuming that they are prepared in a CH_3CN -containing solvent system). Consistent with experiment, our DFT calculations at the M11-L level of theory predict that the free energy of

binding of CH₃CN to the **1^{Phe(H)}** system proceeds with an unfavorable free energy change of +4.9 kcal/mol at 25°C.

Such a weak binding ability of the copper(I) complexes **1^R** toward external substrate was also seen in the treatment with CO, which is a well-known substrate exhibiting strong binding to ordinary copper(I) complexes. For instance, little spectral change was observed upon addition of CO gas to an acetone solution of **1^R** at 25°C, even though CO can form an adduct at very low temperature (-85 °C) as shown in Figure S2. The calculated free energy change for CO binding to **1^{Phe(H)}** was found to be -4.2 kcal/mol assuming standard state conditions (e.g. 1 M CO solution). However, at 25°C the concentration of CO in acetone will be much less than this value, thereby disfavoring binding. At low temperatures, decreased entropic influence and greater CO solubility lead to complexation. Thus, it could be said that our ligands **L^R** highly stabilizes copper(I) complexes with the three-coordinate T-shape structure without any external co-ligand. These structural feature of the copper(I) complexes is somewhat different from that of the Cu_B site of reduced PHM, where the copper(I) center exhibits a distorted four-coordinate tetrahedral geometry with H₂O or CO as the external co-ligand.^{18,71}

Copper(II) Complexes. A series of copper(II) complexes having a different counter anion (**Y**) have been prepared to examine the structural features of the copper(II) complexes supported by ligand **L^R**. The crystal structures of **2^{Phe(NO₂)Cl}** and **2^{Phe(NO₂)OAc}** supported by **L^{Phe(NO₂)}** have already been reported in our previous *Communication*,⁴³ and that of **2^{Phe(NO₂)NO₂}** has been determined in the present study (see Figure S3, Table S3 and S4). The copper(II) complexes of the isopropyl ligand **L^{iPr}** (**2^{iPrCl}**, **2^{iPrOAc}**, **2^{iPrN₃}**, and **2^{iPrNO₂}**) have also been determined in this study (Figure 4), and the crystallographic data and the selected bond lengths and angles are summarized in Tables 3 and 4, respectively. All the copper(II) complexes exhibit a mononuclear structure having the counter anion as an external co-ligand.

The structure of the metal center of **2^{iPrCl}** is essentially the same with that of **2^{Phe(NO₂)Cl}**,⁴³ having a highly distorted tetrahedral geometry with the N₃Cl donor set (Figure 4A). The τ_4 values for **2^{iPrCl}** and **2^{Phe(NO₂)Cl}**, a simple geometry index for four-coordinate

complexes proposed by Houser and his coworkers, are 0.57 and 0.54, respectively; $\tau_4 = [360^\circ - (\alpha + \beta)]/141$, where α and β are the two largest θ angles in the four-coordinate species.⁷² The values of τ_4 will range from 1.00 for a perfect tetrahedral geometry to zero for a perfect square planar geometry.⁷² The isopropyl (iPr) and the phenetyl (Phe(X)) substituents may prevent formation of a Cu₂Cl₂ (doubly chloride-bridged) dimer.

The acetate complex **2^{iPr}OAc** also shows a monomeric structure as in the case of **2^{Phe(NO₂)}OAc**, in which the acetate anion looks like to act as a didentate ligand. However, the distance of Cu–O(2) ($d_{\text{Cu}-\text{O}(2)} = 2.588(3)$ Å) is significantly larger than that of Cu–O(1) ($d_{\text{Cu}-\text{O}(1)} = 1.973(3)$ Å) (Table 4). Thus, the structure of **2^{iPr}OAc** can be regarded as a distorted tetrahedron with the N₃O donor set having a weakly interacting acetate O(2) atom (so-called capped tetrahedron), where τ_4 value is 0.45.

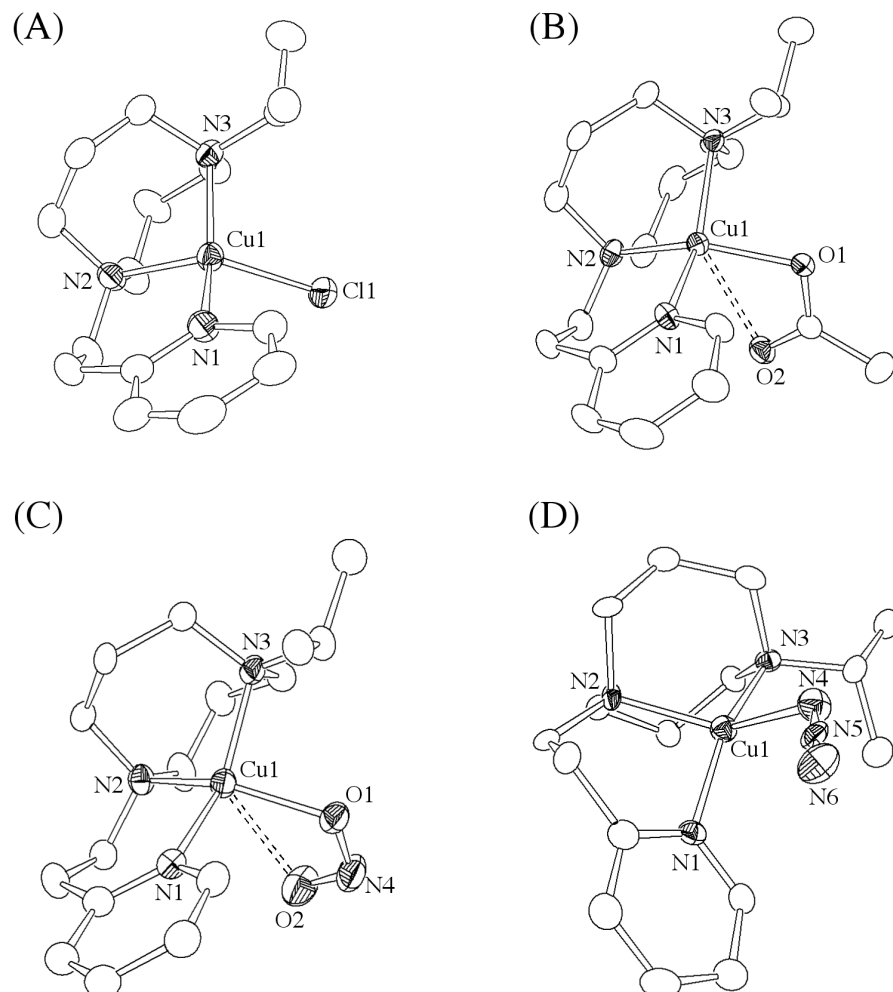


Figure 4. ORTEP drawings of (A) 2^{ipr}Cl , (B) 2^{ipr}OAc , (C) $2^{\text{ipr}}\text{NO}_2$, and (D) 2^{ipr}N_3 showing 50 % probability thermal ellipsoids. The uncoordinated counter anion and the hydrogen atoms are omitted for clarity.

Table 3. X-ray Crystallographic Data of Copper(II) Complexes **2^{iPr}Y**

Compound	2^{iPr}Cl	2^{iPr}OAc
formula	C ₄₀ H ₄₇ BClCuN ₃	C ₁₈ H ₃₀ BCuF ₄ N ₃ O ₂
formula weight	679.64	470.80
crystal system	triclinic	monoclinic
space group	<i>P</i> -1 (#2)	<i>P</i> 2 ₁ /n (#14)
<i>a</i> , Å	11.1894(5)	11.9825(5)
<i>b</i> , Å	11.3597(6)	12.6970(5)
<i>c</i> , Å	14.2362(8)	14.8164(6)
<i>a</i> , deg	103.344(1)	
<i>b</i> , deg	90.250(1)	109.849(2)
<i>g</i> , deg	102.542(1)	
<i>V</i> , Å ³	1715.8(2)	2120.3(1)
<i>Z</i>	2	4
<i>F</i> (000)	718.00	980.00
<i>D</i> _{calcd} , g/cm ³	1.315	1.475
<i>T</i> , K	113	113
crystal size, mm	0.32 x 0.16 x 0.03	0.52 x 0.28 x 0.09
<i>μ</i> (MoKa), cm ⁻¹	7.474	10.833
2θ _{max} , deg	54.9	54.9
no. of reflns measd	16970	20291
no. of reflns obsd	7975 ([<i>I</i> > 1.00σ(<i>I</i>)])	4039 ([<i>I</i> > 1.00σ(<i>I</i>)])
no. of variables	460	310
<i>R</i> 1 ^a	0.0504	0.0566
<i>wR</i> 2 ^b	0.1239	0.1871
GOF	0.997	0.978

^a*R*1 = Σ ||*F*_o|| - ||*F*_c|| / Σ |*F*_o|. ^b *wR*2 = [Σ *w* (|*F*_o²| - |*F*_c²|)² / Σ *w* (*F*_o²)²]^{1/2}

Table 3. X-ray Crystallographic Data of Copper(II) Complexes **2^{iPr}Y** (Continued)

Compound	2^{iPr}NO₂	2^{iPr}N₃
formula	C ₁₆ H ₂₇ BCuF ₄ N ₄ O ₂	C ₁₆ H ₂₇ BCuF ₄ N ₆
formula weight	457.76	453.78
crystal system	orthorhombic	monoclinic
space group	<i>P</i> 2 ₁ 2 ₁ 2 (#18)	<i>Pn</i> (#7)
<i>a</i> , Å	9.7137(6)	7.4111(5)
<i>b</i> , Å	26.834(2)	14.733(1)
<i>c</i> , Å	7.4613(5)	9.2356(6)
<i>a</i> , deg		
<i>b</i> , deg		98.941(1)
<i>g</i> , deg		
<i>V</i> , Å ³	1944.8(3)	996.2(1)
<i>Z</i>	4	2
<i>F</i> (000)	948.00	470.00
<i>D</i> _{calcd} , g/cm ⁻³	1.563	1.513
<i>T</i> , K	103	113
crystal size, mm	0.10 x 0.10 x 0.10	0.24 x 0.21 x 0.06
<i>μ</i> (MoKa), cm ⁻¹	11.800	11.467
2θ _{max} , deg	54.9	54.9
no. of reflns measd	18830	9544
no. of reflns obsd	4450 (All reflections)	7450 ([<i>I</i> > 1.00σ(<i>I</i>)])
no. of variables	280	281
<i>R</i> 1 ^a	0.0538	0.0454
<i>wR</i> 2 ^b	0.1330	0.0732
GOF	1.163	1.047

^a*R*1 = Σ ||*F*_o|| - ||*F*_c|| / Σ |*F*_o|. ^b *wR*2 = [Σ *w* (|*F*_o²| - |*F*_c²|)² / Σ *w* (*F*_o²)²]^{1/2}

Table 4. Selected Bond Lengths (\AA) and Angles (deg) of Copper(II) Complexes 2^{ipr}Y

2^{ipr}Cl			
Cu(1)–N(1)	1.976(4)	Cu(1)–N(2)	1.996(4)
Cu(1)–N(3)	2.036(4)	Cu(1)–Cl(1)	2.2345(11)
Cl(1)–Cu(1)–N(1)	96.54(10)	Cl(1)–Cu(1)–N(2)	131.36(11)
Cl(1)–Cu(1)–N(3)	99.45(10)	N(1)–Cu(1)–N(2)	98.87(16)
N(1)–Cu(1)–N(3)	148.55(14)	N(2)–Cu(1)–N(3)	90.61(15)
2^{ipr}OAc			
Cu(1)–N(1)	2.022(4)	Cu(1)–N(2)	2.000(4)
Cu(1)–N(3)	2.036(3)	Cu(1)–O(1)	1.973(3)
Cu(1)–O(2)	2.588(3)		
O(1)–Cu(1)–N(1)	92.17(12)	O(1)–Cu(1)–N(2)	148.12(13)
O(2)–Cu(1)–N(3)	95.45(11)	O(1)–Cu(1)–O(2)	56.29(10)
N(1)–Cu(1)–N(2)	98.78(14)	N(1)–Cu(1)–N(3)	148.54(14)
N(2)–Cu(1)–N(3)	90.65(13)		
$2^{\text{ipr}}\text{NO}_2$			
Cu(1)–N(1)	2.025(4)	Cu(1)–N(2)	1.980(4)
Cu(1)–N(3)	2.042(3)	Cu(1)–O(1)	2.009(3)
Cu(1)–O(2)	2.513(4)		
O(1)–Cu(1)–N(1)	92.10(13)	O(1)–Cu(1)–N(2)	149.66(14)
O(2)–Cu(1)–N(3)	95.41(13)	O(1)–Cu(1)–O(2)	54.32(12)
N(1)–Cu(1)–N(2)	98.77(14)	N(1)–Cu(1)–N(3)	147.19(14)
N(2)–Cu(1)–N(3)	90.64(13)		

2^{iPr}N₃				
8	Cu(1)–N(1)	1.979(3)	Cu(1)–N(2)	2.024(3)
9	Cu(1)–N(3)	2.016(3)	Cu(1)–N(4)	1.983(4)
10				
11				
12				
13				
14	N(4)–Cu(1)–N(1)	91.85(12)	N(4)–Cu(1)–N(2)	141.73(11)
15	N(4)–Cu(1)–N(3)	94.80(12)	N(1)–Cu(1)–N(2)	95.66(12)
16	N(1)–Cu(1)–N(3)	158.38(11)	N(2)–Cu(1)–N(3)	91.79(11)
17				
18				
19				
20				
21				
22				
23				
24				
25				
26	Recently, Amzel and coworkers reported the crystal structures of PHM soaked with			
27	NaNO ₂ and NaN ₃ . ⁷³ They unambiguously demonstrated that only the Cu _B site of PHM can			
28	bind NO ₂ ⁻ and N ₃ ⁻ anions, consistent with the conclusion that Cu _B is the oxygen- and			
29	substrate-binding site whereas Cu _A is the electron accepter site from ascorbate. ^{17,20} In this			
30	study, the crystal structures of our model compounds 2^{iPr}NO₂ (2^{Phe(NO₂)NO₂}) and 2^{iPr}N₃ were			
31	compared to those of the active sites of the resting state of PHM having NO ₂ ⁻ and N ₃ ⁻			
32	coordinating counter anion.			
33				
34				
35				
36				
37				
38				
39				
40	The overall structure of 2^{iPr}NO₂ is similar to that of 2^{iPr}OAc (Figure 4B), where the			
41	distance of Cu–O(1) ($d_{\text{Cu}-\text{O}(1)} = 2.009(3)$ Å) is much shorter than that of Cu–O(2) ($d_{\text{Cu}-\text{O}(2)} =$			
42	2.513(4) Å) (Figure 4C and Table 4). Thus, the structure of 2^{iPr}NO₂ can also be described as			
43	distorted tetrahedron with a weakly interacting O(2) atom (capped tetrahedron). 2^{Phe(NO₂)NO₂}			
44	exhibits a similar structure to that of 2^{iPr}NO₂ ; $d_{\text{Cu}-\text{O}(1)} = 2.018(4)$ Å and $d_{\text{Cu}-\text{O}(2)} = 2.432(4)$ Å;			
45	(Figure S3). The binding of NO ₂ ⁻ in the Cu _B site of the nitrite-soaked PHM (copper-to-nitrite			
46	oxygen distances are 1.9 and 2.6 Å) is comparable to those of our model compounds. ⁷³			
47				
48				
49				
50				
51				
52				
53				
54	The azide complex 2^{iPr}N₃ also exhibits a mononuclear structure with a highly distorted			
55	tetrahedral geometry having a monodentate N ₃ ⁻ ligand; $d_{\text{Cu}-\text{N}(4)} = 1.983(4)$ Å, $\tau_4 = 0.42$ (Figure			
56	4D). The structural feature of 2^{iPr}N₃ is also similar to that of the Cu _B site in the NaN ₃ -soaked			
57				
58				
59				
60				

PHM; four-coordinate tetrahedral geometry with $d_{\text{Cu-N(4)}} = 2.0 \text{ \AA}$.⁷³ All these results suggest that the copper(II) complexes supported by **L^{iPr}** and **L^{Phe(X)}** are good structure models for the Cu_B site of PHM having the copper(II) oxidation state.

To obtain information about the copper(II) complexes in solution, UV-vis and EPR spectra as well as cyclic voltammetry of **2^{iPr}Y** were measured as summarized in Table 5. The spectra and cyclic voltammograms are presented in Supporting Information (Figure S4 ~ S15).

Table 5. UV-vis Data, EPR Parameters, and Redox Potentials of Copper(II) Complexes **2^{iPr}Y**

complex	λ_{max} (nm) ^a ϵ ($M^{-1} \text{ cm}^{-1}$)	EPR parameter ^b	$E_{1/2}$ (V) ^c	ΔE_p (V)
2^{iPr}Cl	643 (260)	$g_{\parallel} = 2.22$	$A_{\parallel} = 144 \text{ G}$	0.015
	854 (300)	$g_{\perp} = 2.09$		
2^{iPr}OAc	655 (310)	$g_{\parallel} = 2.23$	$A_{\parallel} = 156 \text{ G}$	-0.22
	745 (300)	$g_{\perp} = 2.06$		
2^{iPr}NO₂	650 (340)	$g_{\parallel} = 2.22$	$A_{\parallel} = 160 \text{ G}$	-0.07
	725 (350)	$g_{\perp} = 2.08$		
2^{iPr}N₃	435 (2220)	$g_{\parallel} = 2.22$	$A_{\parallel} = 153 \text{ G}$	-0.03
	643 (690)	$g_{\perp} = 2.09$		
	~780 (shoulder)			

^a In CH₃CN. ^b In acetone. ^c In CH₃CN containing 0.1 M tetra-*n*-butylammonium perchlorate (TBAP) at 25 °C. working electrode glassy carbon, counter electrode Pt, reference electrode Ag / 0.01 M AgNO₃, scan rate 50 mV/s.

The copper(II) complexes exhibit at least two broad and weak d-d bands around 650 nm and above 700 nm (the d-d bands of **2^{iPr}Cl** are exceptionally well separated, see Figure S4), and **2^{iPr}N₃** shows a distinct LMCT band due to the azide ligand at 435 nm (Figure S7). To explore the electronic-structures in detail, TD-DFT calculations employing the hybrid B3LYP density functional and accounting for non-equilibrium solvation were undertaken. The

calculated spectra and the predicted λ_{\max} values for the $\mathbf{2^{iPr}Y}$ complexes were found to be in good agreement with the experimental UV-vis data and were listed in the supporting information along with the description of molecular orbitals involved in the individual excitations (Figures S16–S19 and Tables S5–S8). Analysis of the TD-B3LYP excitations reveals a complex pattern for the broad peaks in the 600~800 nm range whereas the LMCT bands at higher energies could be easily assigned as in the case of $\mathbf{2^{iPr}N_3}$. All of the excitations take place into the same acceptor orbital, which is the lowest unoccupied molecular orbital (LUMO) in the beta manifold but the individual occupied orbitals from which the excitations occur are diverse as illustrated in the supporting information (Tables S5–S8). The LUMOs exhibit significant Cu d character with smaller contributions from π^* orbitals of nitrogen atoms of $\mathbf{2^{iPr}}$ and coordinating atoms of the anionic ligands. For the electronic excitations in the 600~800 nm range, the individual occupied orbitals from which the excitations occur display significant amplitude on Cu centers (and to a lesser amount on $\mathbf{2^{iPr}}$ ligands) as well as on the π^* orbitals of the coordinated anionic ligands. On the other hand, the peaks in the 400~430 nm range for the $\mathbf{2^{iPr}N_3}$ involve electronic excitations from molecular orbitals with mainly $N_3-\pi^*$ character to LUMO orbitals confirming the LMCT assignment.

The EPR spectra of the copper(II) complexes are presented in Figures S8~S11, and the EPR parameters are summarized in Table 5. The complexes exhibit relatively small g_{\parallel} (~2.22) and A_{\parallel} values as compared to those of ordinary copper(II) complexes having tetragonal geometry, suggesting that the tetrahedral distortion of the four-coordinate structure is maintained in solution.

Kitajima and co-workers reported a mononuclear copper(II)-chloride complex supported by HB(3,5-*i*Pr₂pz)₃ [hydrotris(3,5-diisopropyl-1-pyrazolyl)borate] having a tetrahedral geometry.⁷⁴ This compound was, however, easily converted to a five-coordinate copper(II)-Cl complex having additional DMF or DMSO solvent molecule, when the four-coordinate copper(II)-Cl complex was treated with a small amount of DMF or DMSO.⁷⁴ With our copper(II)-chloride complex $\mathbf{2^{iPr}Cl}$, on the other hand, no spectral change was observed even in the presence of large excess (5.0 M) of coordinating solvent such as DMF,

DMSO, and CH₃CN. Thus, the four-coordinate copper(II) complex **2^{iPr}Cl** strongly resists the binding of external fifth ligand. In other words, the copper(II) complexes supported by ligand **L^R** strongly favors the four-coordinate structure.

The copper(II) complexes **2^{iPr}Y** exhibited a quasi-reversible Cu^{II}/Cu^I redox couple ($E_{1/2}$) around 0 V vs Ag/0.01M AgNO₃ in CH₃CN. The slight difference in $E_{1/2}$ among the complexes may be due to the different electronic effects of the coordinating counter anions X.

Formation and Characterization of Copper(II) Superoxo Complex

Reversible O₂-binding to Copper(I) Complex. As we have already reported in the previous *Communication*, the copper(I) complexes supported by the phenetyl derivative **L^{Ph(H)}** reacted with O₂ in a 1:1 ration (determined by manometry) at a low temperature (-85 °C) to produce copper(II) superoxo complexes **2^{Ph(H)}O₂**, exhibiting a characteristic absorption bands at 397 nm ($\epsilon = 4200 \text{ M}^{-1} \text{ cm}^{-1}$), 570 nm (850), and 705 nm (1150) (Scheme 1).⁴³ In this study, essentially the same spectra were obtained in the reactions of other phenetyl derivatives **1^{Ph(X)}** (X = OMe, Me, Cl, and NO₂) and isopropyl derivative **1^{iPr}** with O₂ under the same experimental conditions, demonstrating that the same copper(II)-superoxo complexes **2^{Ph(X)}O₂** (X = OMe, Me, Cl, and NO₂) and **2^{iPr}O₂** were generated in all the ligand systems. A typical example of the UV-vis spectral change for the oxygenation reaction of **1^{iPr}** is shown in Figure 5, where an intense LMCT band at 395 nm ($\epsilon = 5810 \text{ M}^{-1} \text{ cm}^{-1}$) readily appeared together with the broad absorption bands around 585 (980) and 723 nm (1240).

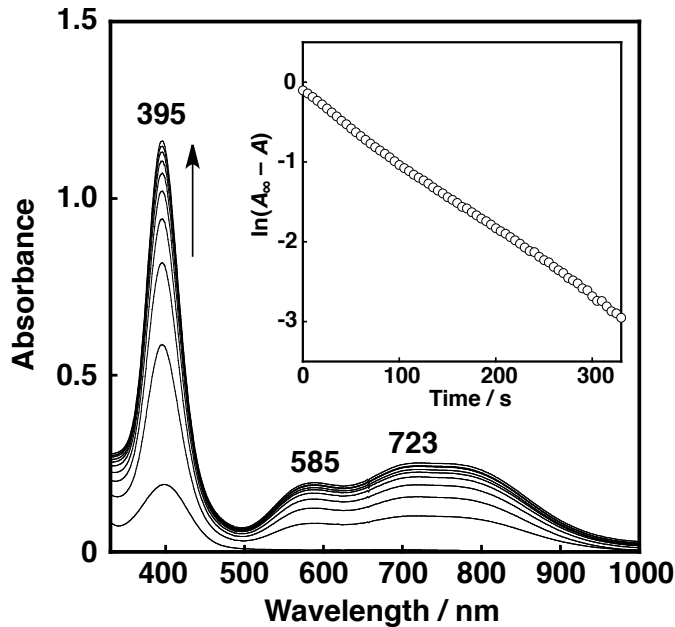


Figure 5. UV-vis spectral change for the oxygenation reaction of $\mathbf{1}^{\text{iPr}}$ (0.2 mM) in acetone at -85°C . Inset: First-order plot based on the absorption changes at 395 nm.

In the resonance Raman spectrum excited at $\lambda_{\text{ex}} = 406.7$ nm, the superoxo complex $\mathbf{2}^{\text{Phe(H)}}\mathbf{O}_2$ exhibited O–O and Cu–O stretching vibrations at 1033 cm^{-1} and 457 cm^{-1} , respectively, which shifted to 968 cm^{-1} and 442 cm^{-1} upon $^{18}\text{O}_2$ -substitution.⁴³ Although the difference spectrum between the $^{16}\text{O}_2$ and $^{18}\text{O}_2$ derivatives clearly indicated the existence of the O–O stretching vibration band, its intensity was significantly weak as compared to the Cu–O band.⁴³ In this study, we have re-examined the resonance Raman spectrum of the superoxo copper(II) species using $\mathbf{2}^{\text{iPr}}\mathbf{O}_2$ (isopropyl derivative) using different excitation laser light at $\lambda_{\text{ex}} = 442$ nm and 647 nm. However, no improvement of the peak intensity was obtained for the O–O stretching vibration band. The O–O moiety of the end-on superoxide ligand may take some different geometries relative to the ligand (\mathbf{L}^{iPr}) backbone, causing the broadening of the Raman peak due to O–O stretching.

The fine-structure EPR study indicated that $\mathbf{2}^{\text{Phe(H)}}\mathbf{O}_2$ has a spin triplet ground state ($S = 1$).⁴³ This assignment is supported by DFT calculations. Theoretical calculations at the M11-L level of theory show that both end-on and pseudo-side-on geometries are possible for $\mathbf{2}^{\text{Phe(H)}}\mathbf{O}_2$ species, with the former isomer being slightly (~ 0.6 kcal/mol) more stable than the latter. For

both isomers, the triplet spin state was found to be the ground state with the singlet structures higher in energy by about 7.0 kcal/mol (Figure S24).

The formation of $\mathbf{2}^{\text{iPr}}\mathbf{O}_2$ shown in Figure 5 follows first-order kinetics in the presence of an excess amount of \mathbf{O}_2 (9.26 mM in acetone at -85°C ; \mathbf{O}_2 concentrations were determined as described in Experimental Section), and the pseudo-first-order rate constant k_{obs} was determined from the first-order plot shown in the inset of Figure 5. Then, the rate-dependence on the \mathbf{O}_2 -concentration was examined as shown in Figure 6, where the plot of k_{obs} against $[\mathbf{O}_2]$ gave a linear correlation with a distinct intercept on the y-axis (Figure 6 shows the rate-dependence on $[\mathbf{O}_2]$ at -90°C . The rate dependence on $[\mathbf{O}_2]$ at -85 , -80 , -75 , and -70°C are shown in Figure S20). Existence of such an intercept in the plot indicates that the \mathbf{O}_2 -binding is reversible (eq 1), and the association rate constant k_{on} and the dissociation rate constant k_{off} of \mathbf{O}_2 are equal to the slope and the intercept, respectively (eq 2).⁷⁵ Reversibility of the \mathbf{O}_2 -binding has been confirmed by the separate experiments demonstrating that \mathbf{O}_2 was removed by bubbling with Ar and/or applying a vacuum and then reforming the superoxo complex by exposure to \mathbf{O}_2 . Then, the equilibrium constant K_{eq} can be determined by eq 3, and the kinetic and thermodynamic parameters were determined from the linear plots of $\ln(k_{\text{on}}/\text{T})$, $\ln(k_{\text{off}}/\text{T})$, and $\ln K_{\text{eq}}$ against $1/\text{T}$ as presented in Figures 7, respectively. The kinetic and thermodynamic parameters for the reactions in THF were determined in the similar manner (Figures S21 and S22), and data are listed in Table 6 together with those of the reactions of $\mathbf{1}^{\text{iPr}}$ in acetone. The kinetic and thermodynamic parameters for the (1 : 1) \mathbf{O}_2 -adduct formation reactions between the copper(I) complexes supported by the tripodal tetradentate ligands tmpa [tris(2-pyridylmethyl)amine] and Me₆tren [tris(2-dimethylaminoethyl)amine] in propionitrile reported by Schindler, Zuberbühler, and coworkers are also included in Table 6.⁷⁶ Similar results for the tmpa system were also reported by Karlin, Zuberbühler, and coworkers.⁷⁷ However, the \mathbf{O}_2 -adduct formation reaction of $\mathbf{1}^{\text{iPr}}$ in propionitrile was too slow, competing with the self-decomposition reaction of generated superoxo complex $\mathbf{2}^{\text{iPr}}\mathbf{O}_2$. Thus, the \mathbf{O}_2 -binding process of $\mathbf{1}^{\text{iPr}}$ in propionitrile could not be examined accurately.

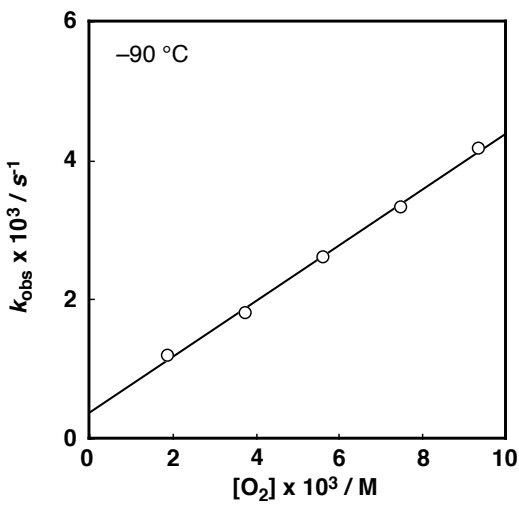
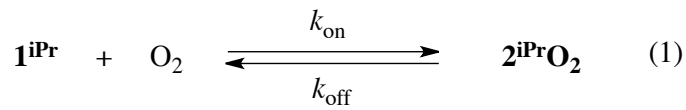


Figure 6. Dependence of the observed first-order rate constant (k_{obs}) on the dioxygen concentration for the formation of $\mathbf{2}^{\text{iPr}}\mathbf{O}_2$ in acetone at $-90\text{ }^{\circ}\text{C}$.



$$k_{\text{obs}} = k_{\text{on}}[\text{O}_2] + k_{\text{off}} \quad (2)$$

$$K_{\text{eq}} = k_{\text{on}}/k_{\text{off}} \quad (3)$$

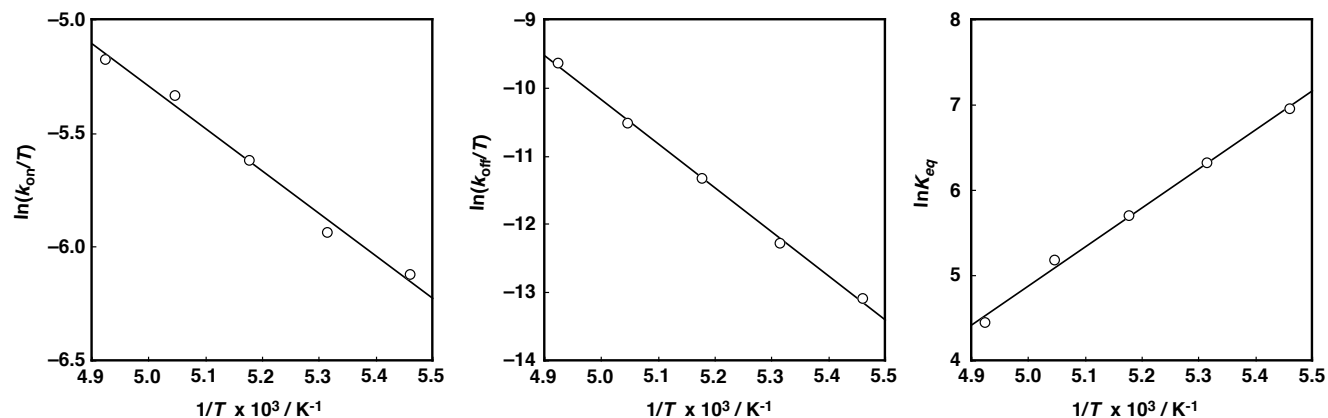


Figure 7. Plots of $\ln(k_{\text{on}}/T)$, $\ln(k_{\text{off}}/T)$, and $\ln K_{\text{eq}}$ vs $1/T$ for the reaction of $\mathbf{1}^{\text{iPr}}$ and O_2 to give $\mathbf{2}^{\text{iPr}}\mathbf{O}_2$ in acetone.

Table 6. Kinetic and Thermodynamic Parameters for the Formation of Copper(II)-Superoxo Complexes (1 : 1-Adduct) upon Low Temperature Oxygenation of Copper(I) Complexes

ligand	solvent	k_{on} (M ⁻¹ s ⁻¹)	activation parameters (k_{on})	k_{off} (s ⁻¹)	activation parameters (k_{off})	K_{eq} (M ⁻¹)	thermodynamic parameters (K_{eq})
L ^{iPr}	acetone	(4.0 ± 0.1) × 10 ⁻¹ (-90 °C)	$\Delta H^{\ddagger} = 15.5 \pm 0.9$ $\Delta S^{\ddagger} = -164 \pm 4.9$	(3.8 ± 0.7) × 10 ⁻⁴ (-90 °C)	$\Delta H^{\ddagger} = 53.5 \pm 1.2$ $\Delta S^{\ddagger} = -14.4 \pm 6.2$	(1.05 ± 0.1) × 10 ³ (-90 °C)	$\Delta H^0 = -38.0 \pm 1.3$ $\Delta S^0 = -150 \pm 6.8$
L ^{iPr}	THF	(7.6 ± 0.2) × 10 ⁻¹ (-90 °C)	$\Delta H^{\ddagger} = 24.4 \pm 1.3$ $\Delta S^{\ddagger} = -110 \pm 6.6$	(1.1 ± 0.1) × 10 ⁻³ (-90 °C)	$\Delta H^{\ddagger} = 33.9 \pm 1.1$ $\Delta S^{\ddagger} = -13 \pm 5.7$	(7.04 ± 0.1) × 10 ² (-90 °C)	$\Delta H^0 = -9.50 \pm 0.31$ $\Delta S^0 = 2.57 \pm 1.6$
tmpa ⁷⁶	EtCN	(1.18 ± 0.01) × 10 ⁴ (-90 °C)	$\Delta H^{\ddagger} = 31.6 \pm 0.5$ $\Delta S^{\ddagger} = 10 \pm 3$	(1.59 ± 0.01) × 10 ¹ (-90 °C)	$\Delta H^{\ddagger} = 61.5 \pm 0.5$ $\Delta S^{\ddagger} = 18 \pm 3$	(7.42 ± 0.04) × 10 ² (-90 °C)	$\Delta H^0 = -29.8 \pm 0.2$ $\Delta S^0 = -108 \pm 1$
Me ₆ tren ⁷⁶	EtCN	(9.5 ± 0.4) × 10 ⁴ (-90 °C)	$\Delta H^{\ddagger} = 17.1 \pm 0.6$ $\Delta S^{\ddagger} = -52 \pm 3$	(7.0 ± 0.3) × 10 ⁻² (-90 °C)	$\Delta H^{\ddagger} = 62.0 \pm 0.6$ $\Delta S^{\ddagger} = 76 \pm 3$	(1.35 ± 0.04) × 10 ⁶ (-90 °C)	$\Delta H^0 = -44.9 \pm 0.2$ $\Delta S^0 = -128 \pm 1$

Units: ΔH^{\ddagger} and ΔH^0 in kJ mol⁻¹ ΔS^{\ddagger} and ΔS^0 in J K⁻¹ mol⁻¹

The association of O₂ to **1^{iPr}** (k_{on} process) in both acetone and THF are significantly slower than those of the copper(I) complexes of tmpa and Me₆tren in propionitrile. In the tmpa and Me₆tren ligand systems, it was suggested that the solvent molecule EtCN binds strongly to the copper(I) ion and thus dissociation of EtCN from the copper(I) complex is rate-limiting for the O₂-adduct formation (dissociative mechanism). This is reflected in the positive or small negative ΔS^{\ddagger} values for tmpa and Me₆tren systems, respectively (Table 6). On the other hand, our ligand system (**L^{iPr}**) exhibits very large negative ΔS^{\ddagger} values both in acetone and THF, suggesting that the association of O₂ to the copper(I) ion is rate-limiting (associative mechanism), and the transition-state structure of the O₂-adduct is highly restricted (Table 6). This is the reason for the much smaller k_{on} values in the **L^{iPr}** ligand system.

With respect to the k_{off} process, the positive ΔS^{\ddagger} values in the tmpa and Me₆tren systems suggest that dissociation of O₂ from the superoxo complex is rate-limiting and resulting copper(I) complex quickly binds to EtCN. This may be due to the stronger binding of the

nitrile solvent to copper(I). On the other hand, the negative ΔS^\ddagger values in the \mathbf{L}^{iPr} system indicate that association of the solvent molecules (acetone and THF) to copper(I) complexes is rate-limiting rather than O_2 -dissociation.

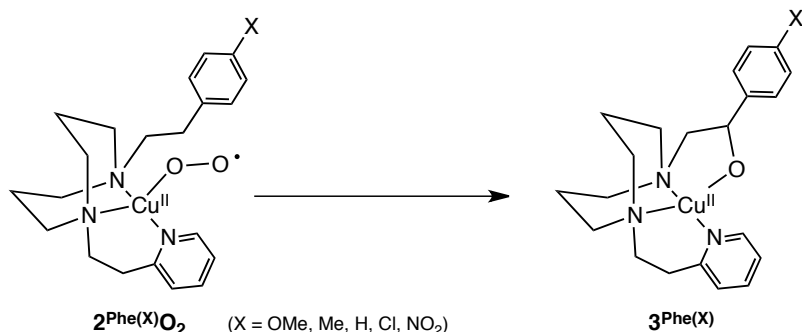
With regard to the thermodynamic parameters, the \mathbf{L}^{iPr} system in THF is exceptional, showing a small negative ΔH^0 and positive ΔS^0 . This clearly indicates that the binding energy of end-on superoxide to copper(II) ion in $\mathbf{2}^{\text{iPr}}\mathbf{O}_2$ is weaker as compared with those in the other systems. This may be due to the existence of some interaction between a THF molecule and the superoxo complex $\mathbf{2}^{\text{iPr}}\mathbf{O}_2$. On the other hand, the thermodynamic parameters in acetone are similar to those of tmpa and Me_6tren ligand systems, where there may be no solvent coordination to the five-coordinate cupric ion in the superoxo copper(II) complexes. This may indicate that there is no solvent coordination to the copper(II) ion in $\mathbf{2}^{\text{iPr}}\mathbf{O}_2$ in acetone neither. The stability of the four-coordinate structure in the copper(II) oxidation state in the present ligand system has been well demonstrated above.

Reactivity of Copper(II) Superoxide Complexes

Aliphatic Ligand Hydroxylation. The copper(II) superoxo complex $\mathbf{2}^{\text{Phe(H)}}\mathbf{O}_2$ has previously been shown to undergo an aliphatic ligand hydroxylation at its benzylic position to give alkoxo-copper(II) complexes $\mathbf{3}^{\text{Phe(H)}}$ (Scheme 3).⁴³ Isotope labeling experiments using $^{18}\text{O}_2$ unambiguously indicated that the oxygen atom of the hydroxyl group comes from molecular oxygen used for the preparation of $\mathbf{2}^{\text{Phe(H)}}\mathbf{O}_2$.⁴³ The $^1\text{H-NMR}$ analysis of organic product obtained by demetalation from the final product complex using NH_4OH (aq) demonstrated that the phenetyl sidearm was hydroxylated in ~35 % yield based on the starting material.⁴³

1
2
3
4
5
6
7
8
9
10
11
12
13
14
15
16
17
18
19
20
21
22
23
24
25
26
27
28
29
30
31
32
33
34
35
36
37
38
39
40
41
42
43
44
45
46
47
48
49
50
51
52
53
54
55
56
57
58
59
60

Scheme 3. Aliphatic Ligand Hydroxylation in End-on Superoxo Copper(II) Complexes $2^{\text{Phe}(X)}\text{O}_2$



In this study, the decomposition (aliphatic ligand hydroxylation) process has been examined in more detail to get mechanistic insight into the C–H bond activation process (Scheme 3). Figure 8 shows the spectral change for the decomposition reaction of $2^{\text{Phe(H)}}\text{O}_2$ at -65°C as a typical example. As clearly shown in the inset of Figure 8, the reaction obeyed first-order kinetics, suggesting that the ligand hydroxylation reaction is a unimolecular (intramolecular) process. The first-order kinetics was further confirmed by the fact that identical first-order rate constants were obtained in the copper concentration range of $0.1 \sim 0.4 \text{ mM}$. The decomposition reactions of all other ligands \mathbf{L}^R also exhibited the first-order kinetics. In the reaction of perdeuterated phenetyl derivative $\mathbf{L}^{\text{Phe(H)}-\mathbf{d}_4}$ (ethylene linker moiety is fully deuterated) appreciable amount of KIE value [KIE = 4.1; $k_{\text{dec(H)}} = 2.5 \times 10^{-4} \text{ s}^{-1}$ and $k_{\text{dec(D)}} = 0.60 \times 10^{-4} \text{ s}^{-1}$] was obtained, indicating that the reaction involves the benzylic C–H bond activation. Furthermore, analysis of the rate-dependence on the reaction temperature (Eyring plot, Figure S23) gives activation parameters for the ligand hydroxylation process as $\Delta H^\ddagger = 19 \pm 0.1 \text{ kJ mol}^{-1}$ and $\Delta S^\ddagger = -223 \pm 0.6 \text{ J K}^{-1} \text{ mol}^{-1}$.

Electronic effects of the *p*-substituent (X) on the hydroxylation reaction were also examined using a series of *p*-substituted phenetyl derivatives $2^{\text{Phe}(X)}\text{O}_2$ (X = OMe, Me, H, Cl, NO₂). The plot of $\log k_{\text{dec}}$ against the Hammett σ_p constants gave a negative small ρ value (-0.63 ; $R = 0.88$) (Figure 9), suggesting that the reactive species exhibits a weakly nucleophilic nature and that the ligand hydroxylation reaction involves hydrogen atom abstraction from the benzylic position of the ligand sidearm.

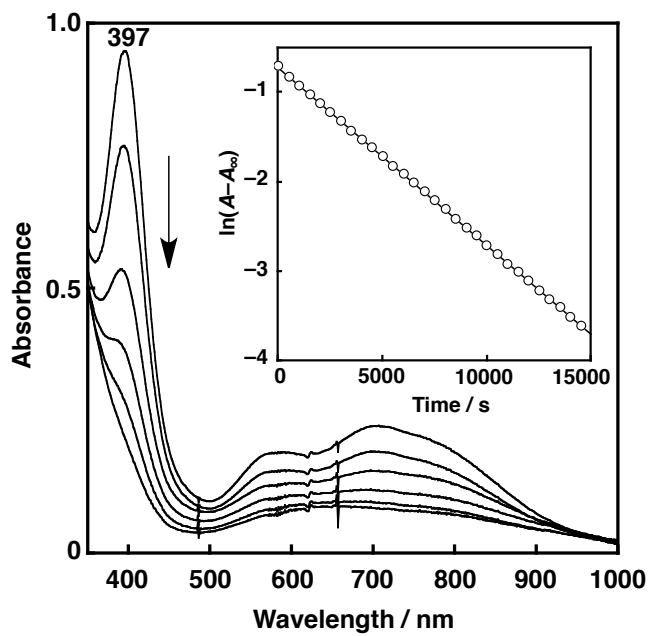


Figure 8. UV-vis spectral change for the decomposition (ligand hydroxylation) of $\mathbf{2}^{\text{Phe(H)}}\mathbf{O}_2$ (0.2 mM) in acetone at -65°C . Inset: Second-order plot based on the absorption changes at 395 nm.

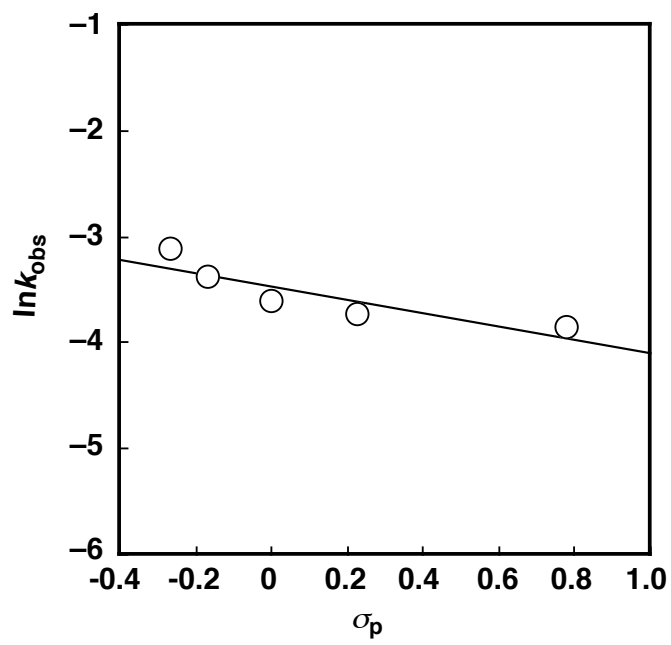


Figure 9. Hammett plot for the ligand hydroxylation in acetone at -60°C .

In order to provide microscopic insight into the details of the mechanistic pathway and various potential intermediates of the ligand hydroxylation, density functional theory (DFT) calculations at the M11-L level of theory were undertaken (see Computational Methods section for full details). To begin, $\mathbf{1}^{\text{Phe(H)}}$ and O_2 were chosen as the reactants and all free energy changes in the proposed mechanisms are reported with respect to separated $\mathbf{1}^{\text{Phe(H)}}$ and O_2 (Figure 10).

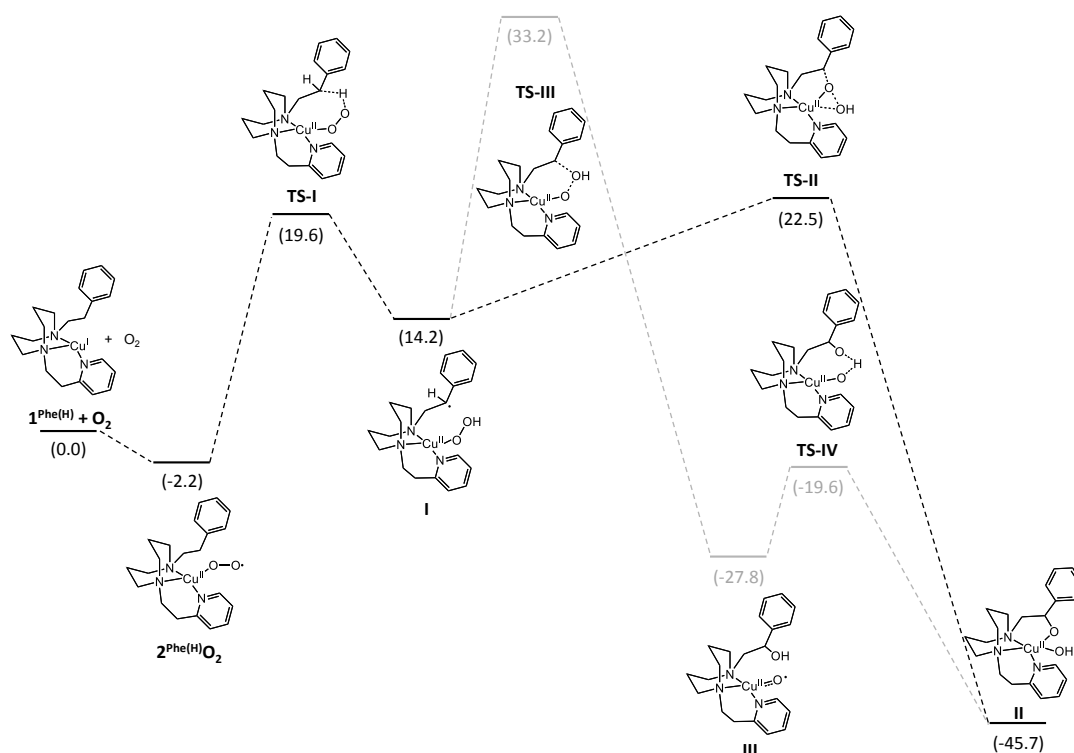


Figure 10. Proposed mechanism for the hydroxylation reaction of $\mathbf{1}^{\text{Phe(H)}}$. Relative free energies at 298.15 K are reported in units of kcal/mol.

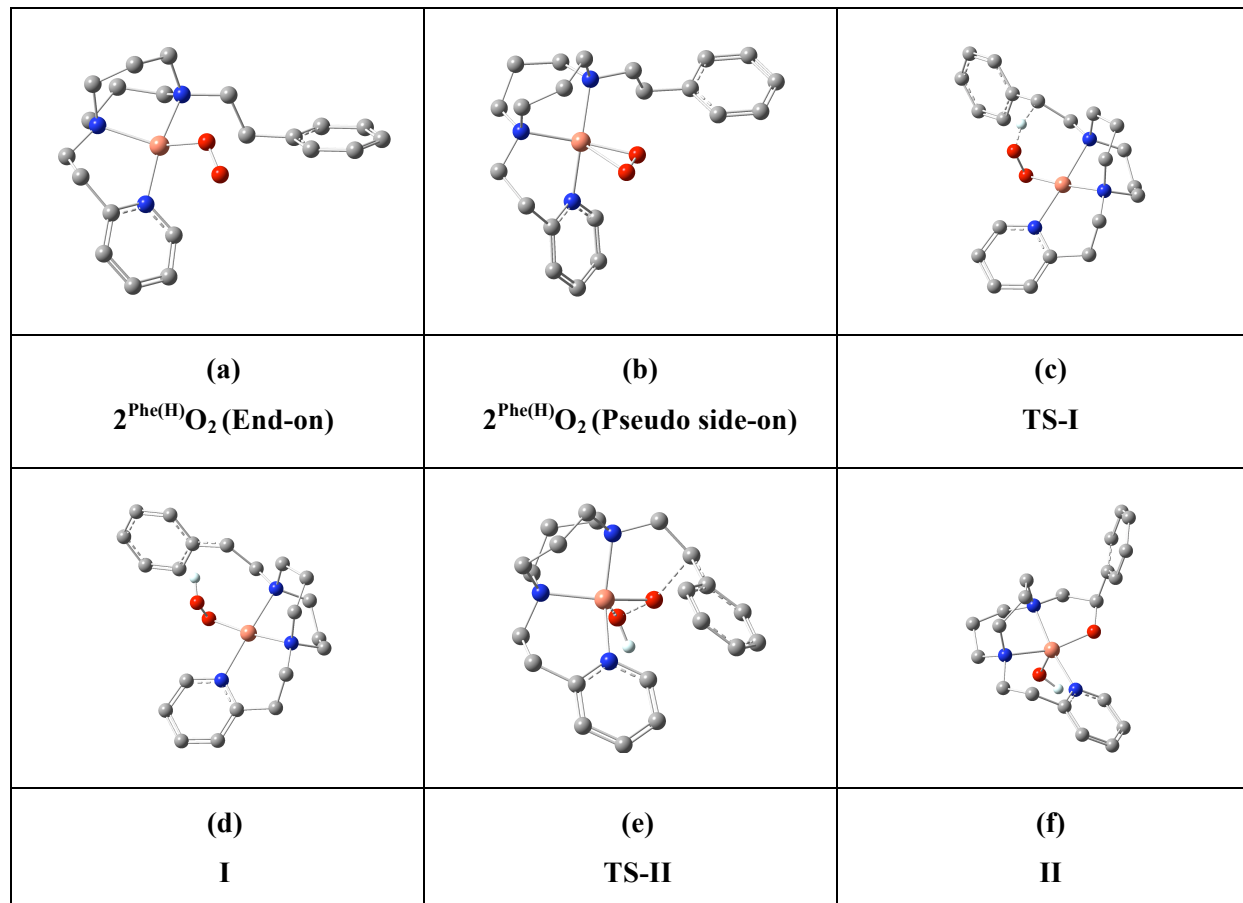
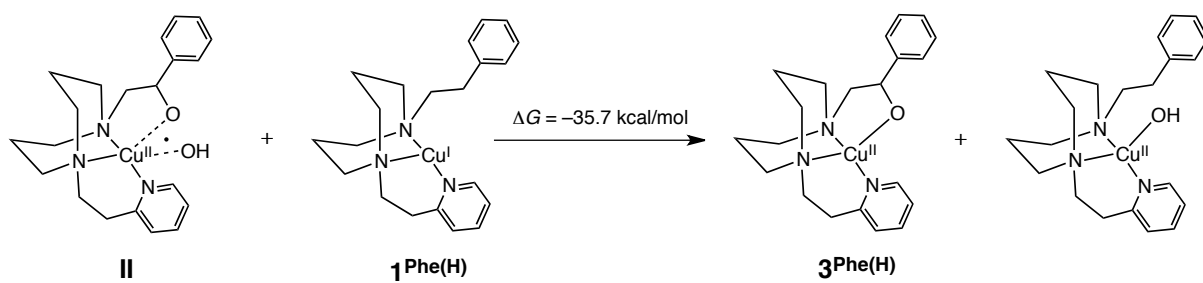
The proposed mechanism for the ligand hydroxylation starts with the formation of $\mathbf{2}^{\text{Phe(H)}}\text{O}_2$ which can be viewed as a copper(II) superoxo complex based on the extent of localized spin density on the copper and oxygen centers. Two conformers, namely end-on and pseudo side-on (Figure 11a and 11b respectively), were located for $\mathbf{2}^{\text{Phe(H)}}\text{O}_2$ that are close in energy, with the end-on structure being slightly more stable (~0.6 kcal/mol). For both

conformers the triplet spin state was found to be the ground state with broken symmetry singlet structures lying about 7.0 kcal/mol higher in energy as stated above.

As a next step, we considered hydrogen atom abstraction from the benzylic position by the copper(II) superoxo unit and we located a transition state structure, **TS-I** (Figure 11c), which has a free energy of activation of 21.8 kcal/mol including tunneling effects.⁷⁸ The resulting intermediate, **I** (Figure 11d), features a copper(II) hydroperoxo complex with a nearby radical center at the benzylic position. Following generation of intermediate **I**, we have identified two possible pathways for the hydroxylation step. Path 1 involves the oxygenation of the benzylic position by the proximal oxygen to the copper center with concomitant O–O bond scission. The located transition state structure on this path, **TS-II** (Figure 11e), has $\Delta G^\ddagger = 8.3$ kcal/mol relative to the preceding intermediate and generates the final product, **II** (Figure 11f). This step is highly exergonic with a free energy change of –59.9 kcal/mol. Path 2 starts with the hydroxylation of the benzylic position by the hydroxo unit of the copper(II) hydroperoxo intermediate **I** also with concomitant O–O bond scission. The free energy of activation associated with the relevant TS structure, **TS-III** (Figure 11g), is 19.0 kcal/mol relative to **I** and the resulting product, **III** (Figure 11h), with hydroxylated benzylic position and a copper(II) oxyl group is 42.0 kcal/mol more stable than **I**. In the final step of this path, the copper(II) oxyl group in intermediate **III** abstracts the hydrogen atom of the hydroxyl group at benzylic position, **TS-IV** (Figure 11i) and generates the same final product **II** as in the first path. This step proceeds with a ΔG^\ddagger of 8.2 kcal/mol relative to **III**. A comparison of the free energy changes indicates that Path 1 is favored significantly over Path 2 as the rate determining step (**TS-II**) in Path 1 has a ΔG^\ddagger of 22.5 kcal/mol compared to 33.2 kcal/mol (**TS-III**) for Path 2, all taken relative to separated reactants. Both pathways lead to the same intermediate **II** which has a triplet ground state and can be described as a supported Cu(II) center with an additional unpaired electron delocalized over the two oxygen atoms. Subsequent reduction of intermediate **II** by unreacted copper(I) complex **1^{Phe(H)}** and hydroxide transfer leads to the formation of the Cu(II)-alkoxide product **3^{Phe(H)}**, a Cu(II)-hydroxide byproduct, and is quite exergonic with a predicted free energy change of

–35.7 kcal/mol (Scheme 4). Invocation of this comproportionation step implies a maximum yield for ligand hydroxylation of 50%. As the redox step follows the rate determining H-atom abstraction step, the second-order character of the redox step does not affect the kinetics.

Scheme 4. Reduction of Intermediate **II** by Copper(I) Starting Material **1^{Phe(H)}**
(The Final Step of the Reaction)



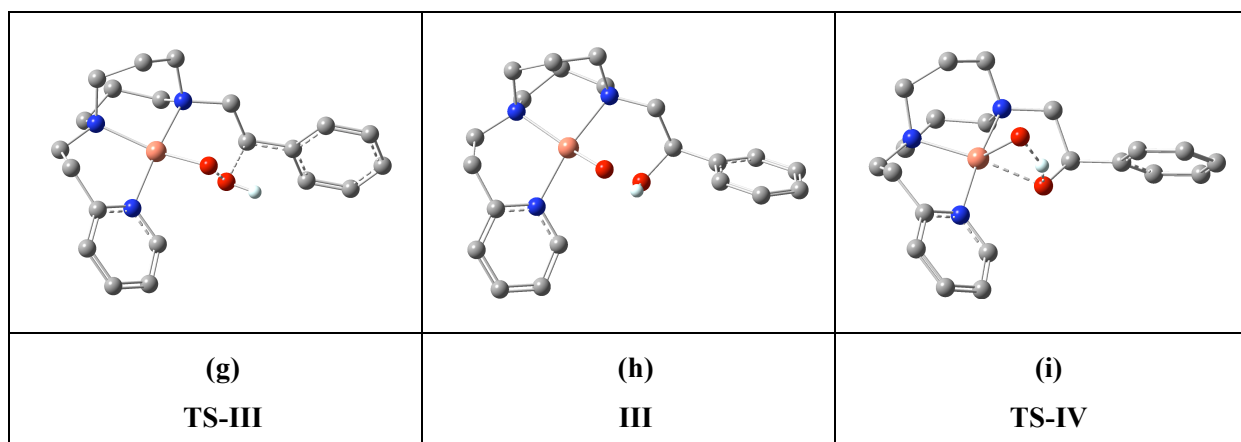


Figure 11. M11-L optimized structures of several complexes potentially relevant to the C–H bond activation reaction mechanism.

In addition to these considerations of the reactions of the mononuclear complex, we also investigated the possible formation and reactivity of dinuclear species. Our calculations indicate that the formation of dinuclear *trans*-peroxo (**4^{Phe(H)}** *trans*-peroxo; this compound has a geometry that is actually intermediate between side-on and end-on peroxy, see Figure S24 of supporting information) and bis- μ -oxo (**4^{Phe(H)} bis- μ -oxo**) species are possible with standard-state ΔG values of -4.5 and 13.0 kcal/mol respectively. The corresponding TS structures for hydrogen atom abstraction from the benzylic positions are associated with ΔG^\ddagger values of 23.1 and 16.4 kcal/mol, respectively (Figure 12). While these absolute values are lower than those predicted for the unimolecular pathway, it must be recalled that these are *standard-state* free energies, and are thus only subject to direct comparison when all species are present at 1 M concentration. As the concentration of **1^{Phe(H)}** is orders of magnitude smaller than 1 mol/L under experimental conditions, the formation and reactivity of dinuclear species is rendered unfavorable, although at much higher concentrations the bis- μ -oxo pathway might well begin to contribute and ultimately dominate the reactivity. In any case, theory is consistent with the observation that the ligand hydroxylation reaction displays first order kinetics an unchanging rate constant over a copper concentration range of $0.1 \sim 0.4$ mM.

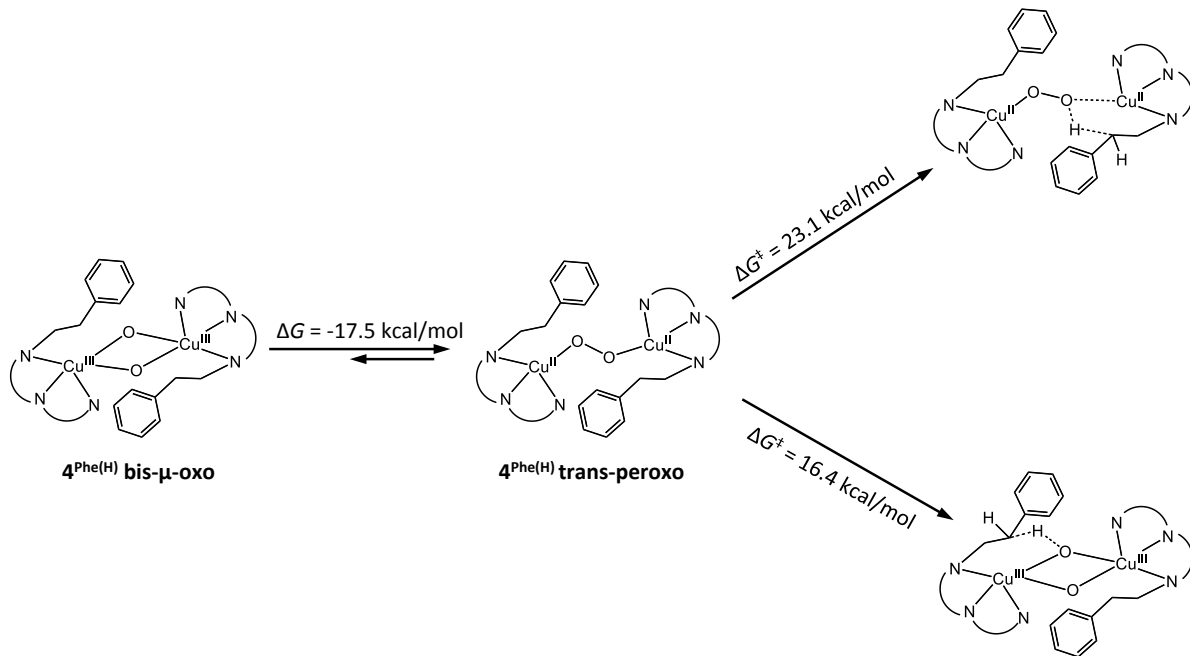


Figure 12. Reactivities of possible dinuclear species, $4^{Phe(H)}$ trans-peroxy and $4^{Phe(H)}$ bis- μ -oxo. The relative free energies at 298.15 K are reported in units of kcal/mol.

Based on these theoretical results, we conclude that ligand hydroxylation proceeds by hydrogen atom abstraction from the benzylic position initiated by the copper(II) superoxo unit of $2^{Phe(H)}\text{O}_2$ followed by oxygenation of the benzylic position by the oxygen proximal to the copper center in **I** with concomitant O–O bond scission. Including an estimation for tunneling effects, we predict a ΔG^\ddagger of 20.9 kcal/mol for the key hydrogen abstraction step by $2^{Phe(H)}\text{O}_2$ and we calculated the KIE for this step to be 5.6 at -65°C , which is in fair agreement with the experimental predictions of about 16.0 kcal/mol for ΔG^\ddagger with a KIE of 4.1. The smaller KIE observed experimentally may indeed be due to some kinetic complexity introduced by the “rebound”-like step of benzylic oxygenation having an activation free energy similar to that for C–H abstraction. At the M-11L level, we predict the rebound to have a somewhat higher

free energy of activation, but the difference of 3 kcal/mol is likely within the error of the various approximations in the theoretical model.

■ CONCLUSION

In this study, structures and physicochemical properties as well as reactivity of the copper(I) and copper(II) complexes supported by the new tridentate ligands L^R have been examined in detail in order to get insight into the chemistry in the active sites of mononuclear copper monooxygenases. The ligand exhibits unique feature to stabilize the copper(I) complexes in a T-shape geometry and the copper(II) complexes in a distorted tetrahedral geometry in the solid state. The copper(II) complexes also favor the four-coordinate structure in solution as demonstrated by the EPR spectra and by the fact that the copper(II) complexes exhibit the same spectra both in the absence and in the presence of highly coordinative solvent such as DMSO and DMF in CH₂Cl₂. Such a distorted tetrahedral structure of the copper(II) complexes resemble to the structure of the Cu_B site of the resting state of PHM.⁷³

Low temperature oxygenation of the copper(I) complexes generated mononuclear copper(II) end-on superoxo complexes having an intense absorption band at ~395 nm and broad bands 585 and 723 nm (Figure 5) and isotope sensitive O–O and Cu–O stretching vibrations of the end-on superoxo species. The superoxo complex has a triplet ground state, which has also been well confirmed by the parallel mode EPR⁴³ and the DFT calculations. Detailed kinetic analysis on the O₂-adduct formation reaction gave the kinetic and thermodynamic parameters providing mechanistic insights into the association and dissociation processes of O₂ to the copper complexes.

The copper(II) end-on superoxo complex gradually decomposes to induce aliphatic ligand hydroxylation to give an alkoxocopper(II) product (Scheme 3). Kinetic studies on the decomposition reaction suggested that the superoxo complex itself is an active species to induce the aliphatic ligand hydroxylation reaction. DFT studies at the M11-L level support that, at low copper concentrations, C–H bond abstraction occurs unimolecularly from the superoxo complex with subsequent rebound of the copper hydroperoxo species to generate an

1
2
3 oxygenated ligand.
4
5

6 To date, the reactivity of several mononuclear copper(II) superoxo complexes has been
7 examined to assess possible involvement of such species in the enzymatic reactions, but none
8 of the superoxo copper(II) model complex has been shown to exhibit direct C–H bond
9 activation of organic substrates.^{37,41,42} Recently, the mononuclear copper(II) superoxo species
10 has been invoked as the key intermediate in the enzymatic reactions catalyzed by PHM and
11 D β M. The present model studies have indicated that such a superoxo species could be
12 reactive enough to induce the direct C–H bond activation of aliphatic substrates.
13
14
15
16
17
18
19
20
21

22 ■ ACKNOWLEDGMENTS

23

24 This work was partially supported by a Grant-in-Aid for Scientific Research on
25 Innovative Areas "Molecular Activation Directed toward Straightforward Synthesis" from the
26 Ministry of Education, Culture, Sports, Science and Technology, Japan (SI, No. 22105007).
27 We are also grateful for financial support from the U.S. National Science Foundation (CJC,
28 MZE, CHE0952054). The authors acknowledge Dr. Minoru Kubo and Prof. Takashi Ogura of
29 University of Hyogo for their help in the trial of resonance Raman measurements of $2^{iPr}O_2$.
30
31
32
33
34
35
36
37

38 ■ REFERENCES

39

- 40
41
42 (1) Klinman, J. P. *Chem. Rev.* **1996**, *96*, 2541-2562.
43
44 (2) Mirica, L. M.; Ottenwaelder, X.; Stack, T. D. P. *Chem. Rev.* **2004**, *104*, 1013-1045.
45
46 (3) Lewis, E. A.; Tolman, W. B. *Chem. Rev.* **2004**, *104*, 1047-1076.
47
48 (4) Chen, P.; Solomon, E. I. *Proc. Natl. Acad. Sci. U. S. A.* **2004**, *101*, 13105-13110.
49
50 (5) Itoh, S. *Curr. Opin. Chem. Biol.* **2006**, *10*, 115-122.
51
52 (6) Cramer, C. J.; Tolman, W. B. *Acc. Chem. Res.* **2007**, *40*, 601-608.
53
54 (7) Roth, J. P. *Curr. Opin. Chem. Biol.* **2007**, *11*, 142-150.
55
56 (8) Rolff, M.; Tuczak, F. *Angew. Chem. Int. Ed.* **2008**, *47*, 2344-2347.
57
58 (9) Punniyamurthy, T.; Rout, L. *Coord. Chem. Rev.* **2008**, *252*, 134-154.
59
60

- (10) Himes, R. A.; Karlin, K. D. *Curr. Opin. Chem. Biol.* **2009**, *13*, 119-131.
- (11) Pap, J. S. n.; Kaizer, J.; Speier, G. *Coord. Chem. Rev.* **2010**, *254*, 781-793.
- (12) Itoh, S. In *Copper-Oxygen Chemistry*; Karlin, K. D., Itoh, S., Eds.; John Wiley & Sons: Hoboken, 2011; Vol. 4, p 225-282.
- (13) Prigge, S. T.; Mains, R. E.; Eipper, B. A.; Amzel, L. M. *Cell. Mol. Life Sci.* **2000**, *57*, 1236-1259.
- (14) Halcrow, M. A. In *Comprehensive Coordination Chemistry II*; Que, J., L., Tolman, W. B., Eds.; Elsevier: Amsterdam, 2004, p 395-436.
- (15) Klinman, J. P. *J. Biol. Chem.* **2006**, *281*, 3013-3016.
- (16) Hess, C. R.; Wu, Z.; Ng, A.; Gray, E. E.; McGuirl, M. A.; Klinman, J. P. *J. Am. Chem. Soc.* **2008**, *130*, 11939-11944.
- (17) Prigge, S. T.; Kolhekar, A. S.; Eipper, B. A.; Mains, R. E.; Amzel, L. M. *Science* **1997**, *278*, 1300-1305.
- (18) Prigge, S. T.; Kolhekar, A. S.; Eipper, B. A.; Mains, R. E.; Amzel, L. M. *Nat. Struct. Biol.* **1999**, *6*, 976-983.
- (19) Evans, J. P.; Ahn, K.; Klinman, J. P. *J. Biol. Chem.* **2003**, *278*, 49691-49698.
- (20) Prigge, S. T.; Eipper, B. A.; Mains, R. E.; Amzel, L. M. *Science* **2004**, *304*, 864-867.
- (21) Bollinger, J., J Martin; Krebs, C. *Curr. Opin. Chem. Biol.* **2007**, *11*, 151-158.
- (22) Francisco, W. A.; Wille, G.; Smith, A. J.; Merkler, D. J.; Klinman, J. P. *J. Am. Chem. Soc.* **2004**, *126*, 13168-13169.
- (23) Bauman, A. T.; Yukl, E. T.; Alkevich, K.; McCormack, A. L.; Blackburn, N. J. *J. Biol. Chem.* **2006**, *281*, 4190-4198.
- (24) Evans, J. P.; Blackburn, N. J.; Klinman, J. P. *Biochemistry* **2006**, *45*, 15419-15429.
- (25) Chen, P.; Solomon, E. I. *J. Am. Chem. Soc.* **2004**, *126*, 4991-5000.
- (26) de la Lande, A.; Parisel, O.; Gérard, H.; Moliner, V.; Reinaud, O. *Chem. Eur. J.* **2008**, *14*, 6465-6473.
- (27) Fujii, T.; Yamaguchi, S.; Funahashi, Y.; Ozawa, T.; Tosha, T.; Kitagawa, T.; Masuda, H. *Chem. Commun.* **2006**, 4428-4430.

- (28) Fujisawa, K.; Tanaka, M.; Morooka, Y.; Kitajima, N. *J. Am. Chem. Soc.* **1994**, *116*, 12079-12080.
- (29) Chen, P.; Root, D. E.; Campochiaro, C.; Fujisawa, K.; Solomon, E. I. *J. Am. Chem. Soc.* **2003**, *125*, 466-474.
- (30) Hong, S.; Huber, S. M.; Gagliardi, L.; Cramer, C. C.; Tolman, W. B. *J. Am. Chem. Soc.* **2007**, *129*, 14190-14192.
- (31) Fujii, T.; Yamaguchi, S.; Hirota, S.; Masuda, H. *Dalton Trans.* **2008**, 164-170.
- (32) Izzet, G.; Zeitouny, J.; Akdas-Killig, H.; Frapart, Y.; Ménage, S.; Douziech, B.; Jabin, I.; Le Mest, Y.; Reinaud, O. *J. Am. Chem. Soc.* **2008**, *130*, 9514-9523.
- (33) Thiabaud, G.; Guillemot, G.; Schmitz-Afonso, I.; Colasson, B.; Reinaud, O. *Angew. Chem. Int. Ed.* **2009**, *48*, 7383-7386.
- (34) Schatz, M.; Raab, V.; Foxon, S. P.; Brehm, G.; Schneider, S.; Reiher, M.; Holthausen, M. C.; Sundermeyer, J.; Schindler, S. *Angew. Chem. Int. Ed.* **2004**, *43*, 4360-4363.
- (35) Würtele, C.; Gaoutchenova, E.; Harms, K.; Holthausen, M. C.; Sundermeyer, J.; Schindler, S. *Angew. Chem. Int. Ed.* **2006**, *45*, 3867-3869.
- (36) Maiti, D.; Fry, H. C.; Woertink, J. S.; Vance, M. A.; Solomon, E. I.; Karlin, K. D. *J. Am. Chem. Soc.* **2007**, *129*, 264-265.
- (37) Maiti, D.; Lee, D.-H.; Gaoutchenova, K.; Würtele, C.; Holthausen, M. C.; Sarjeant, A. A. N.; Sundermeyer, J.; Schindler, S.; Karlin, K. D. *Angew. Chem. Int. Ed.* **2008**, *47*, 82-85.
- (38) Jazdzewski, B. A.; Reynolds, A. M.; Holland, P. L.; Young Jr., V. G.; Kaderli, S.; Zuberbuhler, A. D.; Tolman, W. B. *J. Biol. Inorg. Chem.* **2003**, *8*, 381-393.
- (39) Komiya, K.; Furutachi, H.; Nagatomo, S.; Hashimoto, A.; Hayashi, H.; Fujinami, S.; Suzuki, M.; Kitagawa, T. *Bull. Chem. Soc. Jpn.* **2004**, *77*, 59-72.
- (40) Lanci, M. P.; Smirnov, V. V.; Cramer, C. J.; Gauchenova, E. V.; Sundermeyer, J.; Roth, J. P. *J. Am. Chem. Soc.* **2007**, *129*, 14697-14709.
- (41) Donoghue, P. J.; Gupta, A. K.; Boyce, D. W.; Cramer, C. J.; Tolman, W. B. *J. Am. Chem. Soc.* **2010**, *132*, 15869-15871.

- (42) Peterson, R. L.; Himes, R. A.; Kotani, H.; Suenobu, T.; Tian, L.; Siegler, M. A.; Solomon, E. I.; Fukuzumi, S.; Karlin, K. D. *J. Am. Chem. Soc.* **2011**, *133*, 1702-1705.
- (43) Kunishita, A.; Kubo, M.; Sugimoto, H.; Ogura, T.; Sato, K.; Takui, T.; Itoh, S. *J. Am. Chem. Soc.* **2009**, *131*, 2788-2789.
- (44) Murrayrust, P.; Murrayrust, J.; Clay, R. *Acta Crystallographica Section B-Structural Science* **1980**, *36*, 452-454.
- (45) Houser, R. P.; Young, V. G.; Tolman, W. B. *J. Am. Chem. Soc.* **1996**, *118*, 2101-2102.
- (46) Bu, X. H.; Shang, Z. L.; Weng, W.; Zhang, R. H.; Zhu, H. P.; Liu, Q. T. *Acta Chemica Scandinavica* **1999**, *53*, 295-297.
- (47) Bu, X. H.; Du, M.; Shang, Z. L.; Zhang, R. H.; Liao, D. Z.; Shionoya, M.; Clifford, T. *Inorg. Chem.* **2000**, *39*, 4190-4199.
- (48) Halfen, J. A.; Fox, D. C.; Mehn, M. P.; Que, L. *Inorg. Chem.* **2001**, *40*, 5060-5061.
- (49) Perrin, D. D.; Armarego, W. L. F.; Perrin, D. R. *Purification of Laboratory Chemicals 4th Edition*; 4th ed.; Pergamon Press: Elmsford, NY, 1996.
- (50) Kryatov, S. V.; Rybak-Akimova, E. V.; Schindler, S. *Chem. Rev.* **2005**, *105*, 2175-2226.
- (51) *CRC Handbook of Chemistry and Physics*; CRC Press: New York, 1998; Vol. 79th ed.
- (52) Houser, R. P.; Young, V. G.; Tolman, W. B. *J. Am. Chem. Soc.* **1996**, *118*, 2101-2102.
- (53) Peverati, R.; Truhlar, D. G. *Journal of Physical Chemistry Letters* **2012**, *3*, 117-124.
- (54) Dolg, M.; Wedig, U.; Stoll, H.; Preuss, H. *J. Chem. Phys.* **1987**, *86*, 866-872.
- (55) Hehre, W. J.; Radom, L.; Schleyer, P. v. R.; Pople, J. A. *Ab Initio Molecular Orbital Theory*; Wiley: New York, 1986.
- (56) Frisch et al. Gaussian 09, Revision A.02; Gaussian, Inc.: Wallingford, CT, 2009.
- (57) Cramer, C. J. *Essentials of Computational Chemistry: Theories and Models*; 2nd ed.; John Wiley & Sons: Chichester, 2004.
- (58) Marenich, A. V.; Cramer, C. J.; Truhlar, D. G. *J. Phys. Chem. B* **2009**, *113*, 6378-6396.
- (59) Ziegler, T.; Rauk, A.; Baerends, E. J. *Theor. Chim. Acta* **1977**, *43*, 261-271.
- (60) Noddeman, L. *J. Chem. Phys.* **1981**, *74*, 5737-5743.
- (61) Cramer, C. J.; Truhlar, D. G. *Phys. Chem. Chem. Phys.* **2009**, *11*, 10757-10816.

- (62) Yamaguchi, K.; Jensen, F.; Dorigo, A.; Houk, K. N. *Chem. Phys. Lett.* **1988**, *149*, 537-542.
- (63) Soda, T.; Kitagawa, Y.; Onishi, T.; Takano, Y.; Shigeta, Y.; Nagao, H.; Yoshioka, Y.; Yamaguchi, K. *Chem. Phys. Lett.* **2000**, *319*, 223-230.
- (64) Noddleman, L.; Peng, C. Y.; Case, D. A.; Mouesca, J.-M. *Coord. Chem. Rev.* **1995**, *144*, 199-244.
- (65) Neese, F. *Coord. Chem. Rev.* **2009**, *253*, 526-563.
- (66) Ciofini, I.; Daul, C. A. *Coord. Chem. Rev.* **2003**, *238*, 187-209.
- (67) Harvey, J. N. *Struct. Bond.* **2004**, *112*, 151-183.
- (68) Schmider, H. L.; Becke, A. D. *J. Chem. Phys.* **1998**, *108*, 9624-9631.
- (69) Improta, R.; Barone, V.; Scalmani, G.; Frisch, M. J. *J. Chem. Phys.* **2006**, *125*, 054103.
- (70) The synthetic procedures of $L^{Phe(X)}$ ($X = \text{OMe}$, H , and NO_2) and their copper(I) complexes have already been reported in our previous communication.⁴³
- (71) Boswell, J. S.; Reedy, B. J.; Kulathila, R.; Merkler, D.; Blackburn, N. J. *Biochemistry* **1996**, *35*, 12241-12250.
- (72) Yang, L.; Powell, D. R.; Houser, R. P. *Dalton Trans.* **2007**, 955-964.
- (73) Chufán, E. E.; Prigge, S. T.; Siebert, X.; Eipper, B. A.; Mains, R. E.; Amzel, L. M. *J. Am. Chem. Soc.* **2010**, *132*, 15565-15572.
- (74) Kitajima, N.; Fujisawa, K.; Morooka, Y. *J. Am. Chem. Soc.* **1990**, *112*, 3210-3212.
- (75) Espenson, J. H. *Chemical Kinetics and Reaction Mechanisms*; McGraw Hill, Inc.: New York, 1981.
- (76) Weitzer, M.; Schindler, S.; Brehm, G.; Schneider, S.; Hormann, E.; Jung, B.; Kaderli, S.; Zuberbühler, A. D. *Inorg. Chem.* **2003**, *42*, 1800-1806.
- (77) Zhang, C. X.; Kaderli, S.; Costas, M.; Kim, E.; Neuhold, Y. M.; Karlin, K. D.; Zuberbühler, A. D. *Inorg. Chem.* **2003**, *42*, 1807-1824.
- (78) Skodje, R. T.; Truhlar, D. G. *J. Phys. Chem.* **1981**, *85*, 624-628.